GeoScienceWorld
Lithosphere
Volume 2022, Article ID 9167174, 20 pages
https://doi.org/10.2113/2022/9167174

Lithosphere

Research Article

Spatial Pattern of Late Quaternary Shortening Rate in the Longmen Shan Foreland, Eastern Margin of the Tibetan Plateau

Dawei Jiang, Shimin Zhang, and Rui Ding

National Institute of Natural Hazards, Ministry of Emergency Management of China, Beijing 100085, China

Correspondence should be addressed to Shimin Zhang; shiminzhang@ninhm.ac.cn

Received 28 July 2021; Accepted 25 April 2022; Published 29 May 2022

Academic Editor: Zhikun Ren

As the eastern boundary of the Tibetan Plateau, Longmen Shan possesses a narrow thrust belt with steep topography but lacks matching Cenozoic foreland basin. Multiple kinetic models have been proposed to debate on the dominant mechanism of developing such range–foreland system. Crustal shortening rate is a feasible approach to test different tectonic models and estimate structural patterns. In this study, we focused on the deformation pattern and shortening rate of the complex foreland area of the southern Longmen Shan, which is comprised of the Xiongpo, Sansuchang, and Longquanshan anticlines. By the means of net-based RTK measurement and Quaternary chronology, we measured and dated the six-level terraces of the Qingyi River, which flows southeastward across this region. Excess area method was applied to calculate shortening rate. The results indicate that the Late Quaternary shortening rates of the Xiongpo anticline, Longquanshan anticline, and Sansuchang anticline are 1.01 mm/yr, 0.89 mm/yr, and 0.16 mm/yr, respectively. The total shortening rate of the foreland in southern Longmen Shan is 2.06 mm/yr. Consequently, a mechanical model was presented to show the tectonic pattern: the southern Longmen Shan is an actively expanding edge of the plateau, and the shortening is distributed to the three anticlines dominated by the foreland detachment system. This model supports that crustal shortening is the dominating force in the current orogenesis of the Longmen Shan. In addition, the along-strike variation of the Longmen Shan was further specified from the perspective of crustal shortening distribution. We propose that the southern Longmen Shan and its foreland basin are in a state of compression, while the northern Longmen Shan has both thrust and strike-slip characteristics.

1. Introduction

Longmen Shan is located along the eastern margin of the Tibetan Plateau. In this belt, with the eastward expansion of the plateau, strong oblique shortening happens between the Songpan-Ganzi terrane and Yangtze Craton (i.e., the Sichuan Basin in China) [1, 2]. The dominant mechanism of developing such high topography in the Longmen Shan has been debated continuously. More than six tectonic models that are capable of explaining highly fragmentary geologic and geophysical observations in the thrust belt have been proposed [3, 4]. Some models emphasized the fault-controlled deformation, such as the upper-crustal shortening with a serious of detachments [5–7], the simple-shear or pure-shear shortening and thickening of the lithosphere [3, 4, 8], and the reactivation of preexisting weak zones in the heterogeneous crust [9, 10]. Other models emphasized the large-scale deformation of the crust, such as the channel flow in the mid and lower crust [11, 12], the indentation of the Yangtze Craton [13], and the westward under thrusting of the Yangtze Craton accommodated by distributed shortening in the whole plateau [14]. Among them, the models of upper-crustal shortening and channel flow are treated as end-member models to reveal the fundamental orogenic dynamics. To assess these models, exhumation history [15], tectonic kinematics [10], and deep structure observations [16] have been further studied. Moreover, the Quaternary shortening rate of the Longmen Shan is also significant to the different tectonic models, and the surficial deformation pattern can provide a direct approach to the driving mechanisms. Take the two end-member models, for example; a low crustal shortening rate corresponds to the channel flow model. On the contrast, the upper-crustal shortening model requires a considerable

shortening rate. Therefore, this article focused on the Late Quaternary crustal shortening rate and shortening pattern of the foreland area in the southern Longmen Shan.

After the 2008 Wenchuan earthquake (M_S = 8.0, China Earthquake Networks Center) occurred in the northern range of the Longmen Shan, coseismic data and surface ruptures revealed a distinctive structural pattern, comprised of three primary active faults, including the Wenchuan-Maowen fault, Beichuan-Yingxiu fault, and the Jianyou-Guanxian fault [17, 18]. However, when stretching southward, the pattern becomes a broad thrust zone comprised of six faults, including the Zhonggang fault, Gengda-Longdong fault, Yanjing-Wulong fault, Xiaoguanzi fault, Shuangshi-Dachuan fault, and the Xinkaidian fault (Figure 1). Even during the following 2013 Lushan earthquake (M_S = 7.0, China Earthquake Networks Center), which occurred in the southern range, there were no surface ruptures that could reasonably indicate the overall configuration (Figure 1) [19]. A fold-generated foreland basin is a distinctive feature of the southern range of the Longmen Shan (Figure 1). Unlike the flat Chengdu Plain in front of the northern Longmen Shan, there are two anticlines in the southern section between the Longmen Shan and the boundary of the Cenozoic foreland basin (i.e., the Longquanshan). The tectonic activity of Xiongpo and Sansuchang anticlines is not well constrained [20, 21]. This is mainly because of lush vegetation and intensive weathering.

Tectonic fluvial terraces are substantial features because they can reflect characteristics of mountain uplift and surface deformation [25, 26]. By means of detailed chronology and measurement data, the Quaternary crustal deformation pattern and shortening rate can be obtained through longitudinal profile of river terrace [27–29]. The Qingyi River cuts across the foreland basin of the southern Longmen Shan in a southeastern trend and developed six-level terraces (Figure 1). To avoid elevation uncertainties, a high-precision mobile global positioning satellite (GPS) station with net-based, real-time kinematics (RTKs) was used in the field measurement, its horizontal precision was ±5 cm, and its vertical precision was ±8 cm. A longitudinal profile of Qingyi River terraces was established, which showed Late Quaternary deformation pattern of the foreland area in southern Longmen Shan. Combined with detailed chronology data, including ^{14}C, OSL, and ESR, the regional crustal shortening rate was further calculated. Finally, a kinetic model was established to estimate the deformation pattern and activity distribution of the southern Longmen Shan. In addition, the along-strike variation of the Longmen Shan was further discussed. The main contribution of this work is constraining the Late Quaternary shortening rate of the foreland in southern Longmen Shan.

2. Geological Setting

The Longmen Shan has gradually become the eastern most boundary of the Tibetan Plateau since the collision of the Indian Plate and the Eurasian Plate in 50-60 Ma (Figure 1). The Longmen Shan thrust belt is known for its steep topography and frequent geological disasters [30, 31]. Several studies have been conducted on parts of the mountain belt to show its Quaternary activity [32]. The tectonic of foreland region has been proved to be active during the Quaternary period [21, 33, 34]. Studies on the deep tectonics of the region have indicated that the foreland topography is dominated by thin-skinned structures [33, 35, 36]. Seismic profiles show that branches of the frontal thrust fault have extended into the foreland basin, which suggests the potential for large earthquakes. It can also be seen from the history of large earthquakes between 780 B.C.E. and 2020 C.E. ($M_S \geq 5.0$) that the hypocenters in front of the southern Longmen Shan correspond to the tectonic pattern (Figure 1). In this study, we aim to determine the Late Quaternary activity of the foreland basin in southern Longmen Shan.

As the Cenozoic foreland basin, the Chengdu Plain is located in front of the Longmen Shan. To the east, the Longquanshan anticline is the eastern margin of the range–foreland structure (Figure 1). The northern and southern segments of the active Quaternary structure of the Longmen Shan differ in both their ranges and foreland regions. For instance, in the northern segment, there are three main active thrust faults; from NW to SE, these are Wenchuan-Maowen fault (WMF), Yingxiu-Beichuan fault (BYF), and Guanxian-Anxian fault (JGF, Figure 1) [37]. However, as the three faults stretch southwestward, they grade into at least six active faults, which exhibit minimal evidence of fault activity (Figure 1). Additionally, the detachment fault of the southern Longmen Shan has further extended into the foreland, generating multiple folds, namely, the Xiongpo anticline, the Sansuchang anticline, and the Longquanshan anticline (Figure 2), as well as multiple active faults, including the Datang fault (DTF) and the Pujiang-Xinjin fault (PXF; Figure 2). The Xiongpo anticline was estimated to have experienced an average shortening rate of 0.2 mm/yr since 40–25 Ma. The Xiongpo anticline acted as the deformation front of the Longmen Shan thrust belt between 40 and 25 Ma and 15 and 10 Ma driven by the eastward growth of the Tibetan Plateau [38]. The Datang fault includes a series of steep, east-dipping reverse faults, which roots in a 5–6 km deep basal detachment. It is a younger fault than the northeast-southwest-trending structures in the region. The Pleistocene slip rate on the Datang fault was defined as 0.4-1.2 mm/yr [39].

The southern foreland region has good continuity in its Mesozoic strata, but Cenozoic strata are not well preserved. More specifically, Paleogene sediments are distributed in the north of the Xiongpo anticline only, and Neogene sediments are only distributed on several small massifs along the frontal Longmen Shan (Figures 2 and 3). Additionally, instead of Holocene alluvial sediments, two ancient, abandoned alluvial fans (Q_p) are widely developed and well preserved around the Xiongpo and Sansuchang anticlines (Figure 2(a)). They are also the evidence of strong uplifting of the foreland during the Quaternary period. The GPS velocity field, with a reference of Eurasia, shows the kinematics of the southern Longmen Shan and its foreland (Figure 1) [24]. It can be seen that the foreland region seems to have a similar velocity as the southern Longmen Shan.

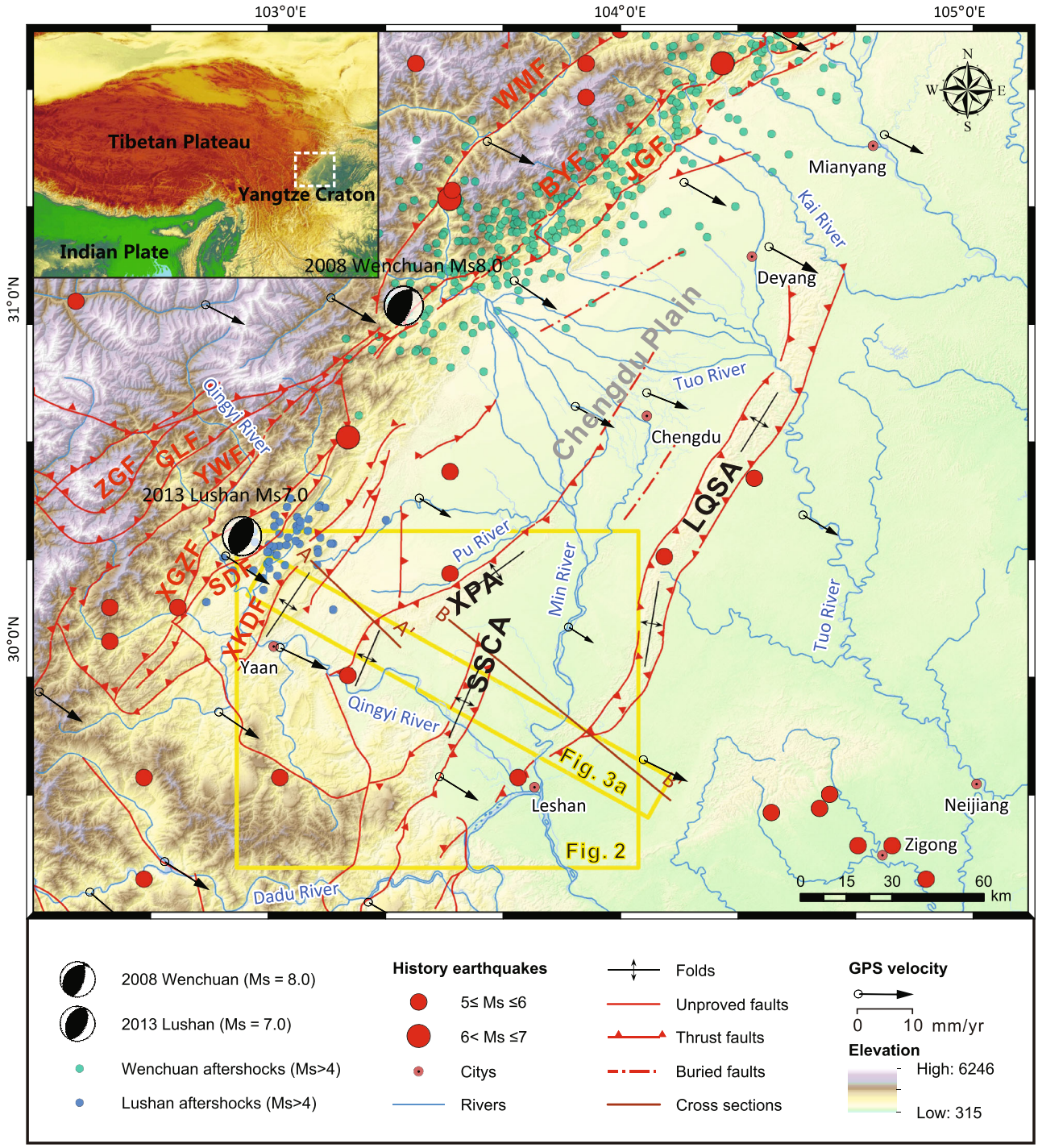

FIGURE 1: Morphological and structural map of Longmen Shan and the Sichuan Basin showing active faults, historical earthquakes, and the global positioning satellite (GPS) field. Focal mechanisms [22, 23] and aftershocks ($M_S \geq 4.0$, Unites States Geological Survey) of the 2008 Wenchuan earthquake and the 2013 Lushan earthquake are projected (small blue dots). Historical strong shocks (780 B.C.E. to 2020 C.E.) are also shown. The GPS velocity field in Eurasian reference frame is drawn as black arrows, showing the kinematics of the southern Longmen Shan [24]. Abbreviations: BYF: Beichuan-Yingxiu fault; JGF: Jiangyou-Guanxian fault; ZGF: Zhonggang fault; GLF: Gengda-Longdong fault; YWF: Yanjing-Wulong fault; XGZF: Xiaoguanzi fault; SDF: Shuangshi-Dachuan fault; XKDF: Xinkaidian fault; LQSA: Longquanshan anticline; SSCA: Sansuchang anticline; WMF: Wenchuan-Maowen fault; XPA: Xiongpo anticline.

A corresponding swath profile was plotted to analyze average topography along the Qingyi River (Figure 3(a), with extent marked in Figure 1). Applied source data was the DEM generated from digital map in the scale of 1 : 50000. Moreover, we drew a geological cross-section and amended it by field surveying to understand the relationship between the surface geology and regional structures (Figure 3). Note that the swath profile (Figures 1 and 3(a)),

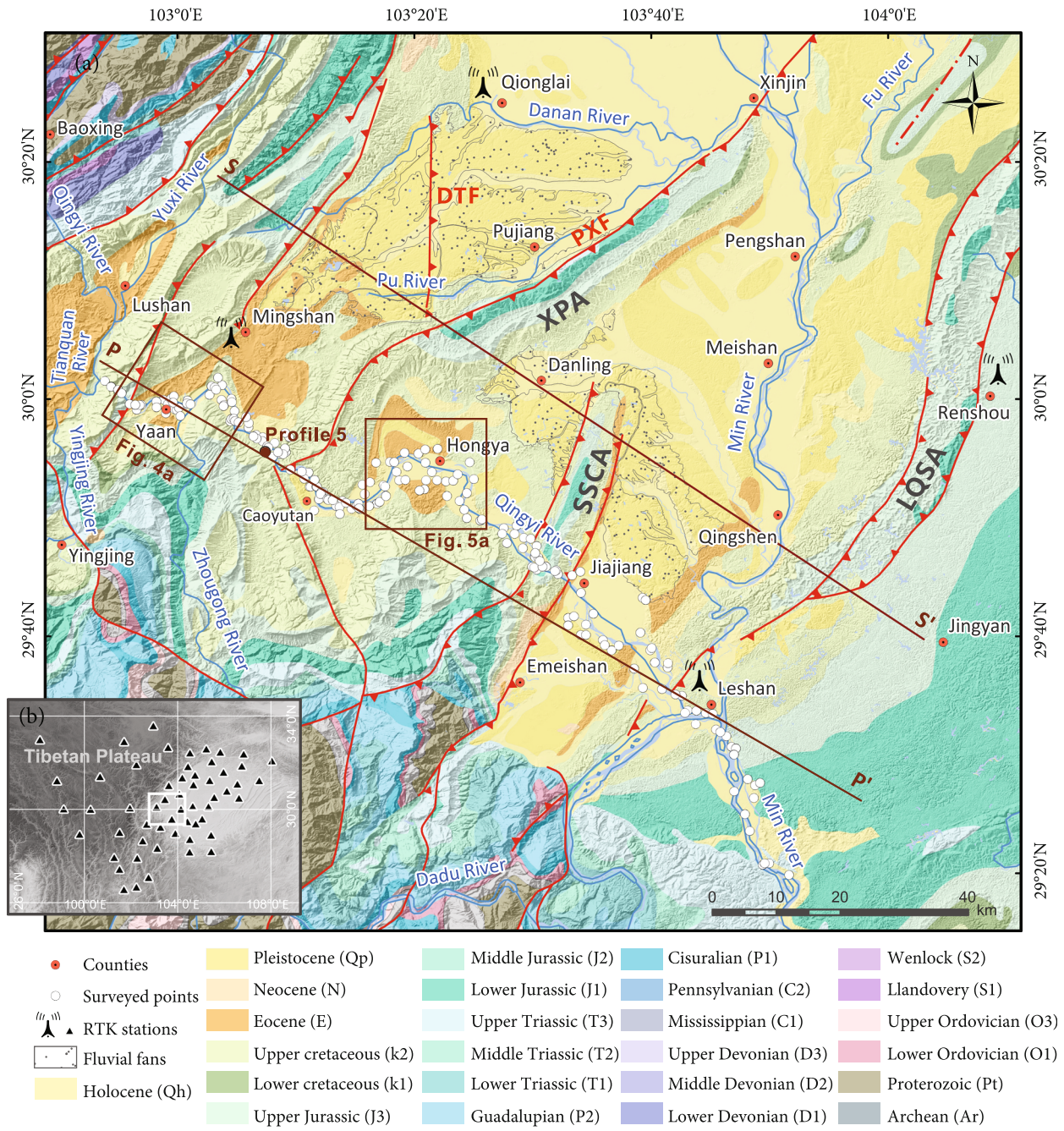

Figure 2: Geological map of the fold-generated region in front of the southern Longmen Shan. (a) Stratum colors follow the Federal Geographic Data Committee (FGDC) standards and (b) network real-time kinematic (RTK) stations of the Sichuan Global Navigation Satellite System (SCGNSS). Locations are from the Sichuan Bureau of Surveying. Symbols and abbreviations are the same as in Figure 1. Abbreviations: DTF: Datang fault; PXF: Pujiang-Xinjin fault.

geological section (Figure 3(b); profile S-S′ in Figure 2), and the seismic profiles (Figure 3(c); profiles A-A′ and B-B′ in Figure 1) were not strictly corresponded. We selected the position of geological profile to reveal more stratum information. We considered the diver position and adjusted them to each other in the final analysis. In view of the topographic features, as the boundary of the foreland basin, the Longquanshan is the longest anticline in front of the Longmen Shan thrust belt, which stretches for ~200 km (Figure 1). However, in the southern foreland, the Xiongpo anticline is more prominent than the Longquanshan, which can be clearly seen from a swath profile (Figure 3(a)). Additionally, the Sansuchang anticline is relatively low, and its core has been strongly eroded, showing relatively weak activity. The deformation of river terrace shows a trend similar to that of the topography.

We investigated the deformation of Qingyi River terraces to reveal the activity of the southern foreland basin. The Qingyi River is the largest river in the southern Longmen Shan. It flows through the range from the county of Baoxing

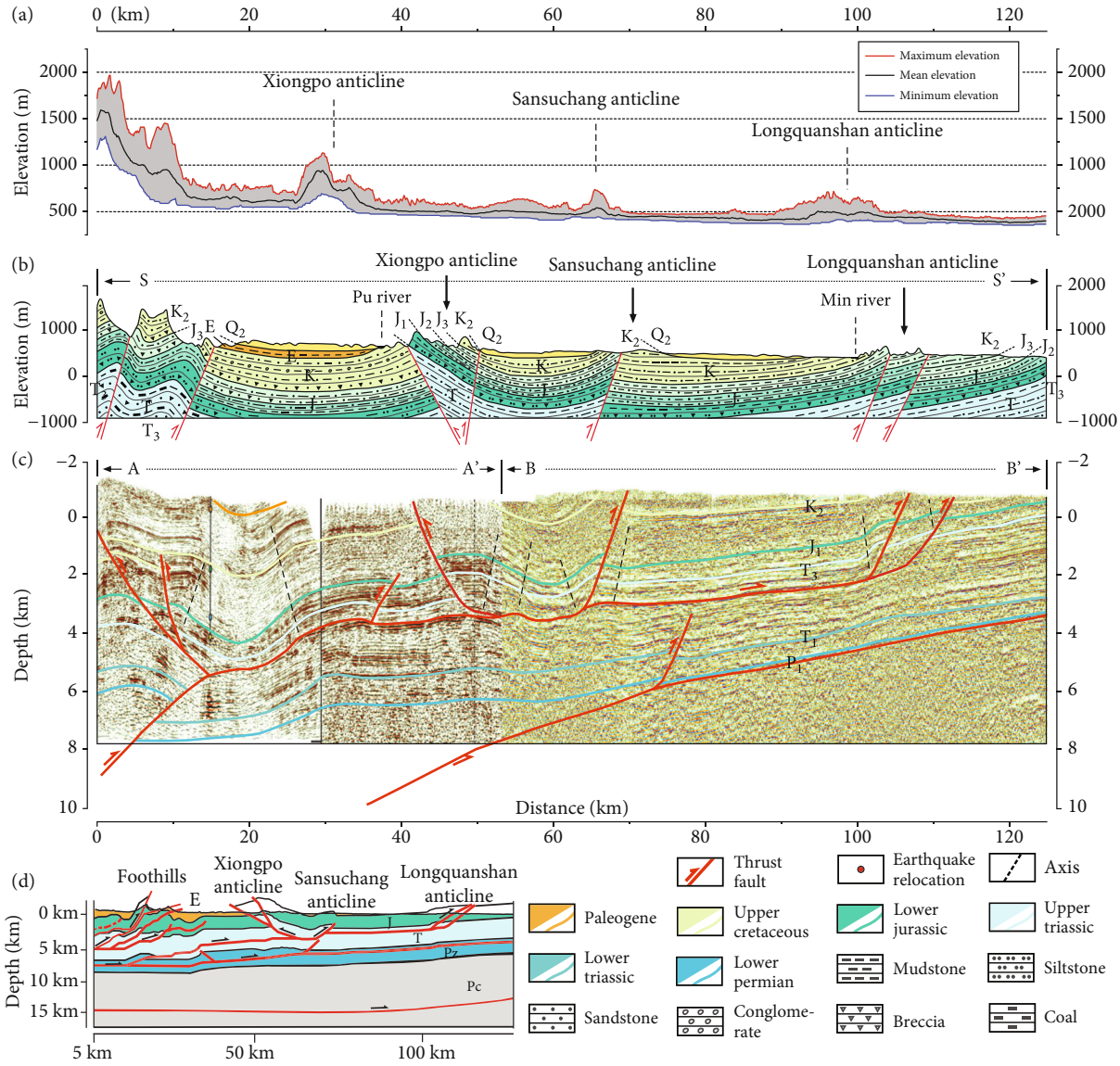

Figure 3: Geomorphological and tectonic characteristics of the study area. (a) Swath profile of the foreland basin (area shown in Figure 1); the width and length of the swath profile were 15 km and 125 km, respectively. (b) Geological cross-section showing the setting of Mesozoic and Cenozoic strata in the foreland basin (S-S′, position shown in Figure 2). (c) Seismic section of the foreland basin (A-A′ and B-B′, locations shown in Figure 1), in which the interpretation of the A-A′ and B-B′ sections follows the studies of Li et al. and Wang et al. [16, 36, 40]. (d) Deep structures of the southern Longmen Shan and its foreland basin [5]. Colors of the strata follow the FGDC standards. Symbols and abbreviations are the same as in Figure 2.

upstream to Ya'an City downstream (Figure 2(a)). Finally, it reaches the trunk of the Yangtze River in Leshan City, along with the Min River and Dadu River (Figure 2(a)). Accordingly, the Qingyi River is a reasonable feature for studying the Quaternary activity of the foreland area in southern Longmen Shan.

3. Methodology

3.1. Measuring and Surveying Terraces. Using the deformation of terraces to interpret active tectonics, precision of longitudinal profile is one of the most important factors. Under the conditions of kilometer-scale surveying, RTKs can provide accurate data and have been widely applied. RTK surveying is usually based on Bluetooth or wireless network technologies, which have a distance limit of ~5 km. However, in the measurement of the 150 km long Qingyi River, traditional RTKs cannot provide continuous and accurate mapping results. To solve this problem, we used a net-based RTK approach, using the Sichuan Global Navigation Satellite System (SCGNSS). The SCGNSS was constructed by the Chinese government following the Wenchuan M_S 8.0 earthquake in 2008 in order to replenish the destroyed surveying facilities. It is now composed of 60 satellite stations (Figure 2(b)), which can provide real-time modifying functions to the survey work across the eastern margin of the Tibetan Plateau. Additionally, there are three stations in the research area: Qionglai station, Mingshan station, and Leshan station (Figure 2(b)). Thus,

we can achieve an altitudinal survey precision of ±8 cm with the SCGNSS across the entire Qingyi River basin. During the study, we measured all terrace surfaces and their straths along the Qingyi River. The terraces in different levels were investigated in the field. Every measured terrace was estimated to be originally developed. The overlap layers including flood sediments, depositions of barrier lake, or sediments formed by human activities were all excluded. All data were measured under the coordinate system of the UTM Northern Hemisphere 48. Then, the data were projected along a 120-degree axis vertical to regional structures in contrast with topography and seismic profiles. The measured points were marked on the geological map (Figure 2).

3.2. Classifying Fluvial Geomorphology. The sequence of river terraces is the base of establishing the longitudinal profiles. In order to define the sequence of river terraces, we initially classified the terraces according to the heights above the riverbed and the marker layer. However, because of the heavy weathering caused by the humid climate, the terraces developed in the study area are fragmentary. We encountered difficulties in accurately distinguishing among terraces in multiple levels. Meanwhile, during the field survey, we found that the matrix of terrace sediments obviously varied from one another. The weathering of old terraces seemed to be more serious than the young ones, which may be related with the climate. Overall, the different weathering can help to classify the terraces in different ages. Therefore, we applied bulk element testing to help accounting for the degrees of weathering of different-level terraces. Sedimentary samples belonging to each terrace were collected, and terraces with thick, silty, top deposits were excluded, as these may be young overbank deposits. To avoid excessive erosion, the samples were collected at a depth of ~2 m beneath the terrace surface. Bulk and trace element analyses were then applied to reveal the degree of weathering. Testing was completed at the Key Laboratory of Crustal Dynamics of the China Earthquake Administration. The classification of terraces is a detailed process of fundamental work. Hence, the results and analyses of bulk and trace elements were shown in Supplemental material E.

3.3. Dating Terrace Formation Ages. The age of the terraces studied varied from thousands of years to the Middle Pleistocene. Therefore, multiple dating methods were used. Carbon isotope dating (^{14}C) was applied to terrace T1 (youngest); optical stimulated luminescence dating (OSL) was applied to terraces T1, T2, and T3, and electron spin resonance dating (ESR) was used for terraces T4, T5, and T6 (oldest). The samples were collected in the sand or clay layer close to the top fluvial gravels, as we attempted to approach the age of the morphological surface of the terrace. Totally, four samples of terrace T1 (including two ^{14}C and two OSL samples), six samples of terrace T2 (OSL samples), two samples of terraces T3 (OSL samples), three samples of T4 (ESR samples), one sample of T5 (ESR sample), and one sample of T6 (ESR sample) were collected and dated in the laboratory. Carbon isotope samples were dated at the School of Archaeology and Museology, Peking University; OSL samples were dated at the Key Laboratory of Crustal Dynamics, China Earthquake Administration, and ESR samples were dated at the State Key Laboratory of Earthquake Dynamics, China Earthquake Administration.

3.4. Estimating Crustal Shortening by Morphometry. To calculate the regional crustal shortening rate, a model with a clear tectonic structure must first be established. We combined the surficial terrace deformation with the deep structures to interpret tectonic pattern and calculate regional crustal shortening rate. The longitudinal profile of terraces' elevations was transformed into terraces' heights above the riverbed to show deformation in detail and correlate to deep structures. We applied the Monte Carlo simulation to estimate uncertainties of the increments in evaluating the terrace ages and calculating of crustal shortening rates. In our simulations, the probability distributions of each input parameter are sampled randomly for 50000 trials to generate a frequency distribution. Reported values reflect the mode of the output histogram and the associated 95% confidence intervals. Input parameters contain the excess area, detachment depth, and terrace age. Output parameters contain the total shortening length and shortening rate. Details of the Monte Carlo simulation are shown in Supplemental material D.

4. Results

4.1. Investigation of Terraces at Multiple Levels. In the foreland region of the Longmen Shan, six terraces are preserved formed during different stages of the Quaternary period along the Qingyi River; in age-ascending order, they are T1, T2, T3, T4, T5, and T6. Among them, terraces T1–T4 are distributed along the entire length of the river. Terraces T5 and T6 are only developed around the Ya'an region. Here, we take the Ya'an Valley (i.e., Ya'an City) and Hongya Valley (i.e., Hongya Town) as examples to introduce the terrace details.

4.1.1. Terraces in the Ya'an Valley. In the Ya'an Valley, the heights of the leading edges of the terraces above the modern riverbed are ~4.9–8.5 m for T1, ~15.2–18.6 m for T2, ~48.0–59.9 m for T3, ~88.1–92.1 m for T4, ~130.1–150.8 m for T5, and~204.3–209.1 m for T6 (Figures 4(a) and 4(b)). Terrace T6 is preserved only at the top of Longgang Mountain, southwest of Ya'an City (Figure 4(a), profile 6). The visible sedimentary strata area is 5.6 m thick, and the thickness of the gravels above the bedrock strath is 11.2 m (Figure 4(c)). The terrace sediments are comprised of quartzite and mudstone gravels, with diameters ranging from 8 to 35 cm. The matrix between the gravels is clay. Terrace T5 is preserved along the Qingyi River between Ya'an City and the town of Hongya, mainly north of the Xiongpo anticline (Figure 4 (a), profile 5). The thickness of the sediments in profile is 11.5 m (Figure 4(c)). Gravels in the outcrop are comprised of quartzite, sandstone, and mudstone, with a small amount of magmatic rocks. The matrix between the gravels has been weathered into clays (Figure 4(c)). Terrace T4 is mainly developed on the piedmont, south of the Ya'an Valley (Figure 4(a), profile 4). In profile 4, a 3.8 m thick brownish

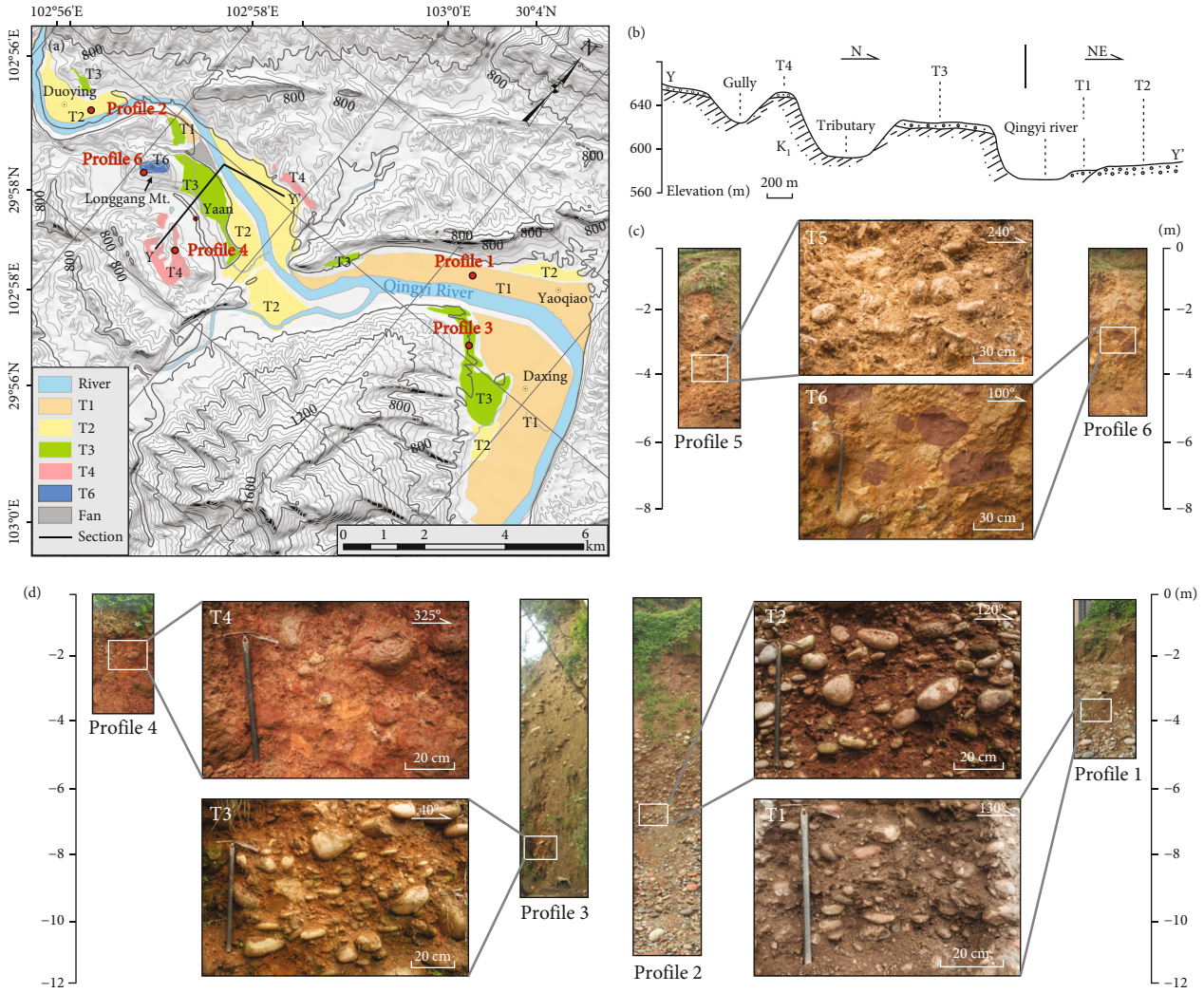

FIGURE 4: Distribution and sedimentary characteristics of the Qingyi River terraces in the Ya'an Valley. (a) Distribution of the terraces in the Ya'an River Valley (extent shown in Figure 2(a)); (b) field-measured Y-Y′ cross-section (locations shown in (a)); (c) outcrops of terraces T5 and T6, and the locations of the profile are shown in Figures 2(a) and 3(a), respectively; and (d) outcrops of terraces T1–T4 (locations shown in (a)).

red sandy clay layer mixed with gravel can be seen (Figure 4 (d)). The gravels are mainly comprised of sandstone and lesser amounts of quartzite, and the matrix is weathered to a brownish red clay (Figure 4(d)). Terrace T3 is distributed mainly from Ya'an City to the town of Jiajiang (Figure 4 (a), profile3). In profile 3 (Figure 4(d)), the gravel layer is 18.5 m thick. The matrix between the gravels is brown, clayey sand (Figure 4(d)). Terraces T2 and T1 are distributed along the entire Qingyi River Valley. In profile 2 (Figure 4), the matrix is comprised of reddish brown sand and silt. Additionally, the gravels in T1 and T2 are barely weathered, and the matrix holds the original structure, with coarse particle sizes.

4.1.2. Terraces in the Hongya Valley. In the Hongya Valley, the heights of the leading edges of the terraces above the modern riverbed are ~6.5–8.6 m for T1, ~21.4–25.6 m for T2, ~73.9–81.5 m for T3, and ~127.2–132.3 m for T4 (Figures 5(a) and 5(b)). Terraces T1-T4 in the Hongya Valley are all basin-wide distributed. Terrace T4 is distributed around the highest hills along the river. The thickness of the gravels above the bedrock strath of T4 is 20.5 m. The sediments are comprised of quartzite and mudstone gravels, with diameters ranging from 10 to 30 cm. The matrix between the gravels is clay (Figure 5(c)). Terrace T3 is distributed more limited, and its gravel layer is 16.5 m thick. Gravels in the outcrop are comprised of quartzite, sandstone, and mudstone. The matrix between the gravels is brown, clayey sand (Figure 5(c)). Terraces T2 and T1 are distributed along the entire Hongya Valley. Gravels in the outcrop are mainly comprised of sandstone and mudstone. The matrix is comprised of reddish brown sand and silt (Figure 5(c)).

4.1.3. Longitudinal Profile of the Terraces. Terraces of Qingyi River are discontinuously distributed in the study area. Hence, we acquired the altitudes of riverbed and terraces T1–T6 via mobile surveying. All the riverbed and terrace

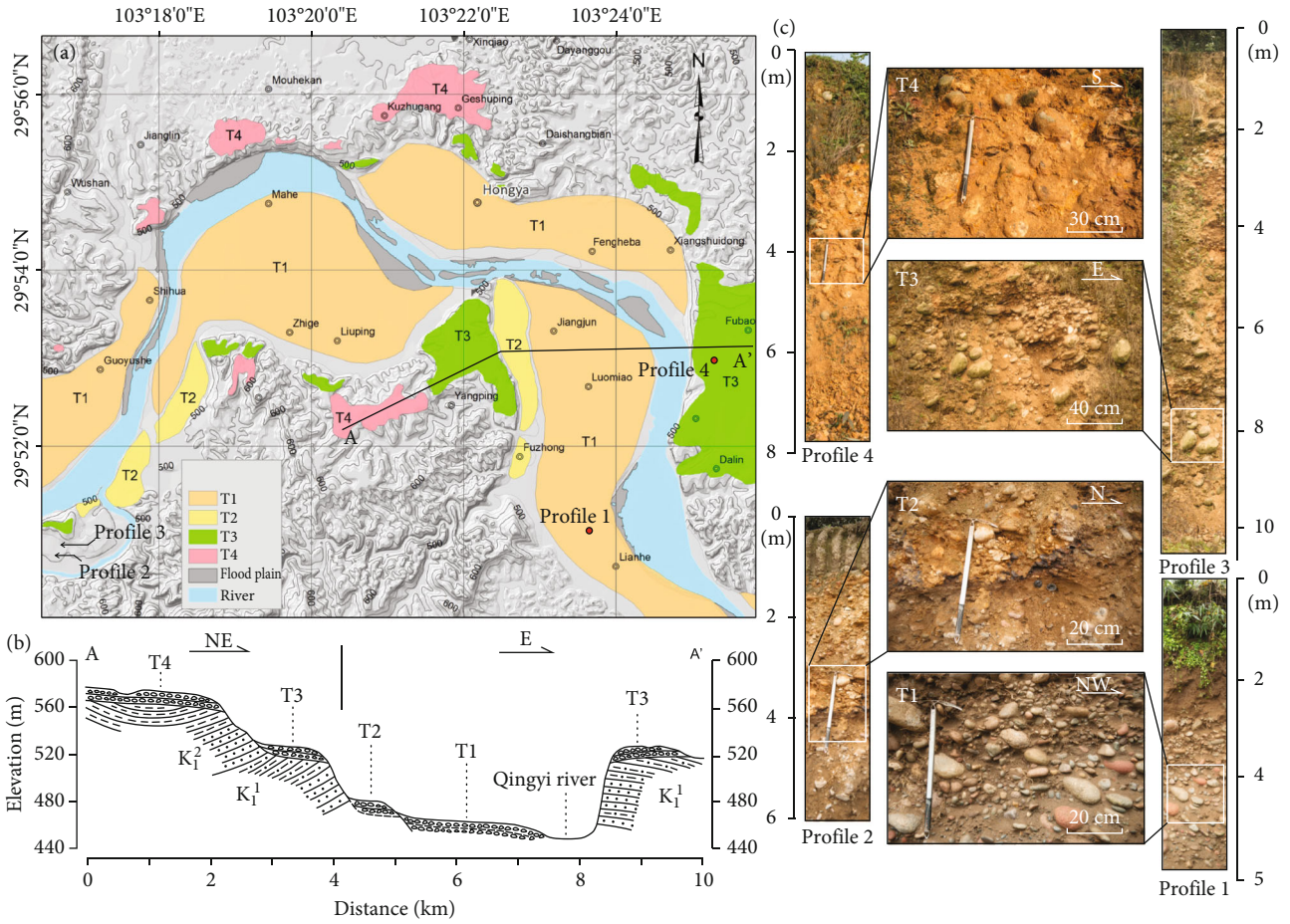

FIGURE 5: Distribution and sedimentary characteristics of the Qingyi River terraces in the Hongya Valley. (a) Distribution of the terraces in the Hongya River Valley (extent shown in Figure 2(a)); (b) field-measured A-A′ cross-section (location shown in (a)); and (c) outcrops of terraces T4, T3, T2, and T1 (locations shown in (a)).

points were measured individually with a mobile GPS based on network RTKs (see Section 3.1). Considering that there were many villages on the terraces, we tried to measure the initial terrace surfaces and corresponding straths. To reduce the influence of river bends, all the measurement data were projected to the tectonic line P-P′, which is vertical to the strikes of the Longmen Shan and foreland anticlines (Figures 2 and 6(b)). In view of the plotted longitudinal profile (Figure 6(a)), the deformation of Xiongpo anticline was reflected by terraces in all levels. It can be seen that the basin-wide terraces T1–T4 show distortions to differing extents around the anticlines. Terraces T6 and T5 have been seriously eroded, but in view of the trend of T5's surface, the Xiongpo anticline may have had the same activity before the period of T4, which promoted the damage of high terraces around the anticline (Figure 6(a)). Near the Xiongpo and Longquanshan anticlines, a new local terrace, T1b, has developed because of recent uplift, but T1b is absent around the Sansuchang anticline (Figure 6(a)). Around the Longquanshan area, terraces T4 and T3 were all eroded, and only terraces T2 and T1 can reflect tectonic activities (Figure 6(b)). The original RTK measurement data are listed in the Supplemental material F.

4.2. Terrace Chronology. Multiple dating methods were employed to test terrace samples, which are distributed in the town of Lushan, upstream of the Qingyi River, Ya'an City in the midstream, and the town of Hongya downstream (Figure 7). Carbon isotope dating (^{14}C) was applied to terrace T1; optical stimulated luminescence dating (OSL) was applied to terraces T1, T2, and T3, and electron spin resonance dating (ESR) was used for terraces T4, T5, and T6. To approach the age of the morphological surface of the terrace, the samples were collected in the sand or clay layer close to the top fluvial gravels as far as possible. All chronology samples were collected in newly excavated outcrops to avoid of pollution. The details of the outcrops that used to collect dating samples are listed in supplemental material A.

4.2.1. Dating Results of ^{14}C. Original dating results are listed in Table 1, and the radiocarbon results were calibrated with the software package OxCal [41]. The detailed calibrated results are shown in Supplemental material B.

4.2.2. Dating Results of OSL. Detailed chemical data of the samples are shown in Table 2, including the contents of

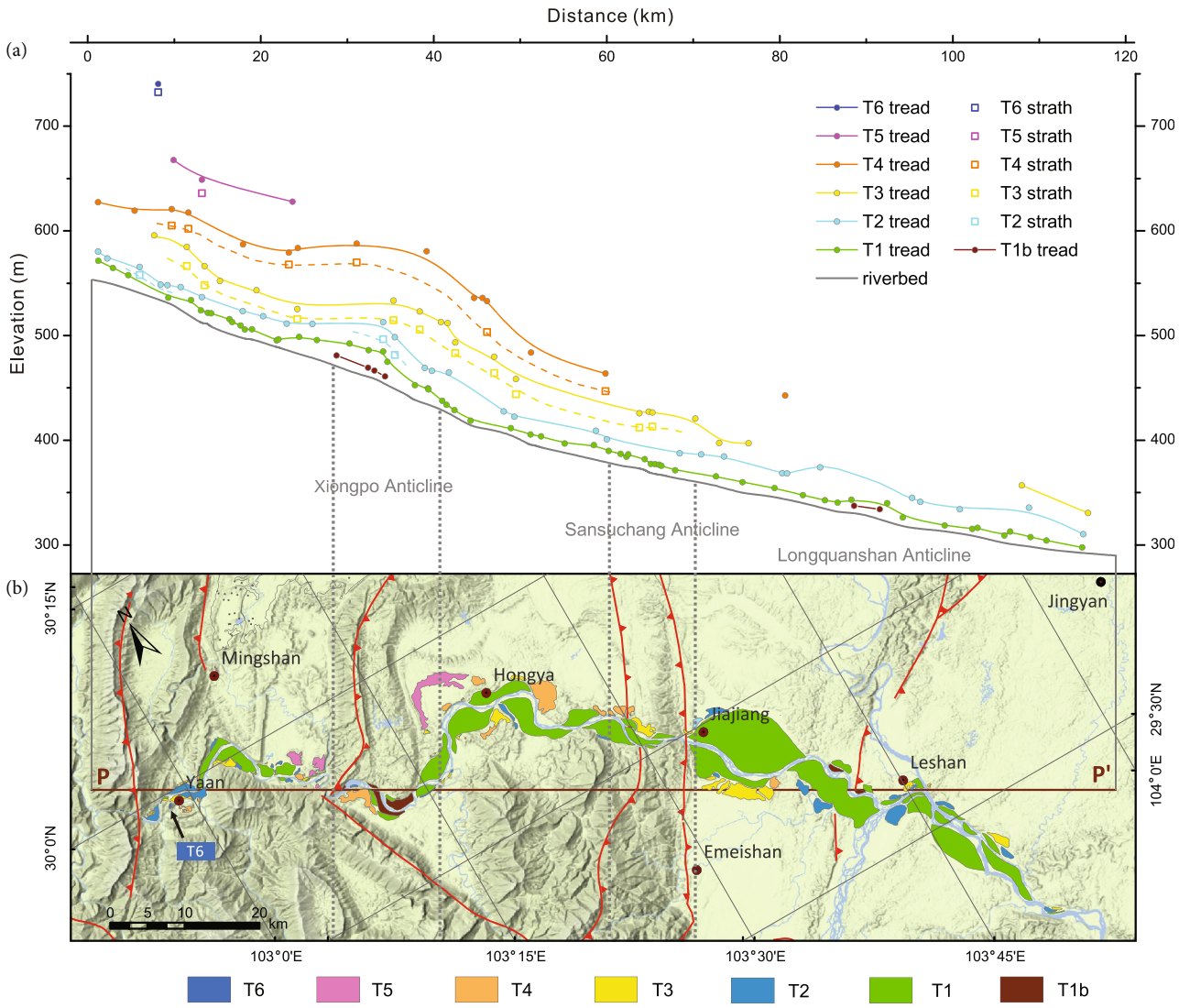

FIGURE 6: Longitudinal profile of Qingyi River terraces, including terraces T1–T6. (a) Deformation of terraces near anticlines; (b) distribution of T1–T6 terraces along the projection axis, P-P′. The location of P-P′ is also shown in Figure 2(a). Symbols and abbreviations are the same as in Figure 1.

U, Th, and K, the testing grain size, environmental dose, and the equivalent dose of the samples. The simplified multiple aliquot regenerative (SMAR) dose protocol [42] was applied. Additionally, the OSL signals and sensitivity-corrected OSL of each sample are shown in Supplemental material C.

4.2.3. Dating Results of ESR. The chemical data during sample testing are listed in Table 3.

4.2.4. Geochronological Summary. The revised test results are listed in Figure 8 and Table 4. Through the results, it can be seen that the terraces are approximately isochronous (Figure 8 and Table 4), especially terraces T1, T2, T3, and T4. Although the Qingyi River is reported to have migrated for several times [43], the river channel should has not changed since the development of terrace T4. Accordingly, it should be reasonable to use the deformation of terraces at the same level to solve tectonic problems. Notably, among the ages of terraces T2 and T3, ages of the terraces in the mountain area of Ya'an and Lushan differ from that in the campaign area. Through the field survey, we consider that the formation of terrace in the mountain area is steady and continuous. The main misleading factor is the overlap layers caused by large floods, which may lead to excessively young ages. In the downstream area, the river channel sways within a specific range and leads to complex depositions. So, we decided to exclude excessive age results of terrace T2 from the calculation of the rate of shortening. As to terrace T3, we did not get sufficient results to evaluate distribution characteristic of the ages. Compared with the ages of terraces T2 and T4, we consider that the result of 73.1 ± 9.7 ka was extremely young and was not applied in the final calculation of shortening rates. In the evaluation of the terrace ages, we

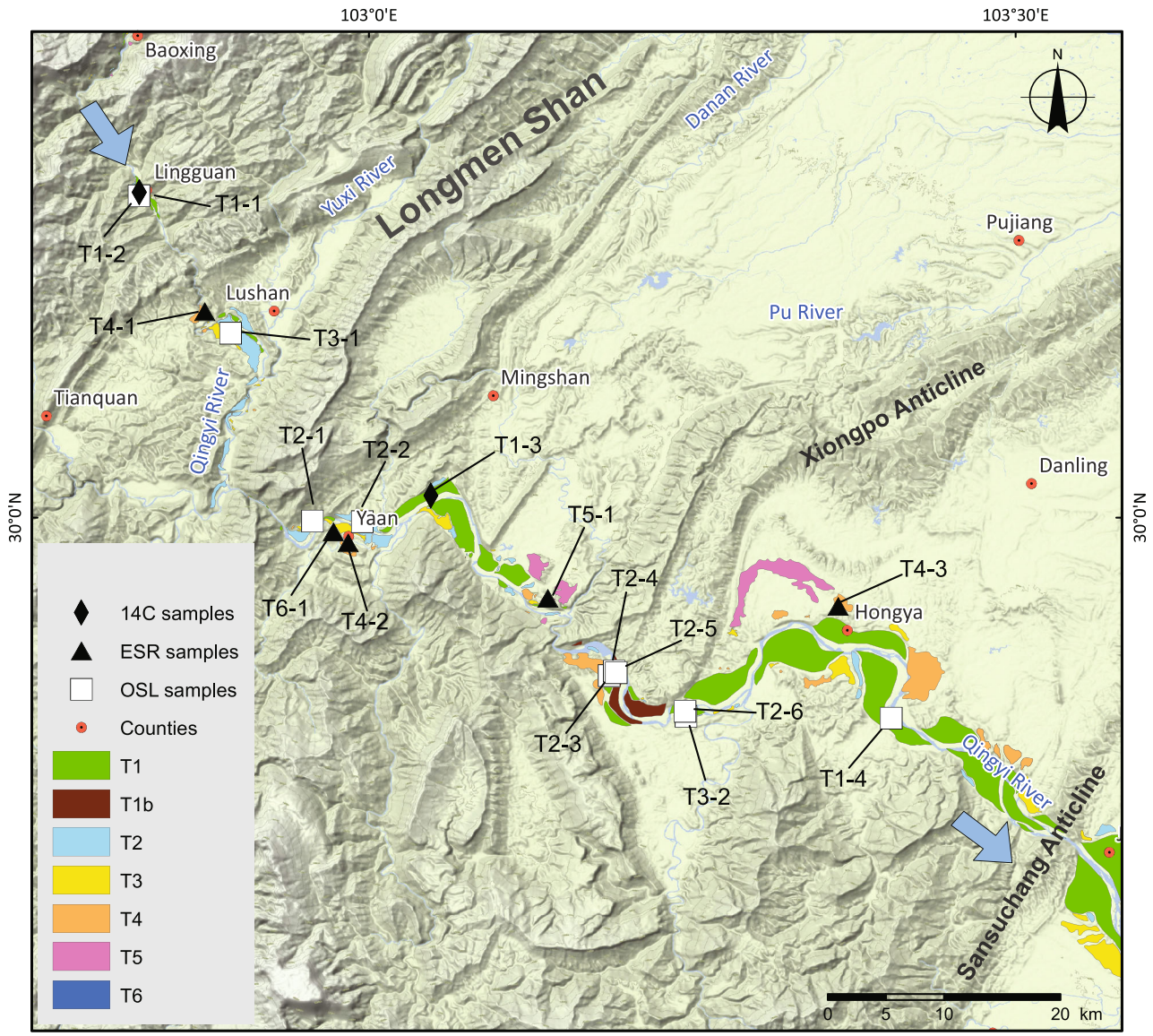

Figure 7: Distribution of chronology samples along the Qingyi River basin.

Table 1: Radiocarbon (^{14}C) test results.

Samples	Sites	Coordinates (WGS 84)	Radiocarbon age (yr)	Calibrated result (Cal B.C.)	Calibrated result (Cal B.P.)
T1-1	Lushan	30°15′3.03″ 102°49′22.35″	6020 ± 20	4981–4845	6931–6795
T1-3	Ya'an	30°1′1.39″ 103°2′52.65″	5910 ± 30	4844–4715	6794–6665

applied the Monte Carlo simulation method to avoid the increase of error. In the simulations, the probability distributions of each ages were sampled randomly for 50000 trials to generate a frequency distribution.

4.3. Shortening Rate in the Longmen Shan Foreland. To calculate the regional crustal shortening rate, a model with a clear tectonic structure must first be established. We combined the surficial terrace deformation with the deep structures to interpret tectonic pattern and calculate regional crustal shortening rate (Figure 9). The longitudinal profile of terraces' elevations was transformed into terraces' heights above the riverbed to show deformation in detail (Figure 9). It can be seen that the deformation pattern of river terrace is influenced by anticline uplifting (Figure 8(b)), especially those of the Xiongpo and Longquanshan anticlines. In addition, there is a deficiency of Paleogene strata between these anticlines, which are locally preserved in front of the

Table 2: Optical stimulated luminescence (OSL) test results.

Sample	U (μg/g)	Th (μg/g)	K (%)	Grain size (μm)	Moisture content	Environment dose (Gy/ka)	Equivalent dose (Gy)	Age (ka)
T1-2	3.64	17.90	2.43	4~11	25.75	4.74	36.2 ± 2.1	7.6 ± 0.9
T1-4	0.94	7.00	1.76	4~11	5.92	3.03	20.4 ± 1.4	6.8 ± 0.8
T2-1	2.61	13.10	2.33	4~11	14.22	4.49	181.2 ± 13.1	40.4 ± 5.0
T2-2	1.58	8.14	1.88	4~11	11.60	3.33	134.5 ± 12.9	40.4 ± 5.6
T2-3	1.00	8.48	1.74	4~11	14.12	2.93	167.6 ± 17.1	57.1 ± 8.2
T2-4	1.33	8.05	1.88	4~11	18.78	2.99	159.7 ± 13.7	53.5 ± 7.0
T2-5	1.07	6.92	1.70	4~11	21.74	2.49	172.5 ± 21.9	69.4 ± 11.2
T2-6	1.40	10.30	1.93	4~11	20.40	3.23	218.0 ± 34.5	67.5 ± 12.6
T3-1	2.20	11.70	1.72	4~11	12.85	3.70	270.4 ± 23.8	73.1 ± 9.7
T3-2	1.81	11.20	1.87	4~11	18.28	3.52	356.1 ± 39.3	101.3 ± 15.1

Table 3: Electron spin resonance (ESR) test results.

Samples	U (μg/g)	Th (μg/g)	K_2O (%)	Moisture content	Paleodose (Gy)	Annual dose (Gy/ka)	Age (ka)
T4-1	2.60	11.7	2.15	39.14	582 ± 93	2.2	163 ± 26
T4-2	4.31	18.8	2.26	22.7	662 ± 70	3.6	185 ± 19
T4-3	2.47	13.0	1.17	31	358 ± 35	1.9	185 ± 18
T5-1	3.68	18.8	2.51	33.9	622 ± 124	2.9	217 ± 43
T6-1	1.58	7.07	2.00	31.40	602 ± 120	2.0	300 ± 60

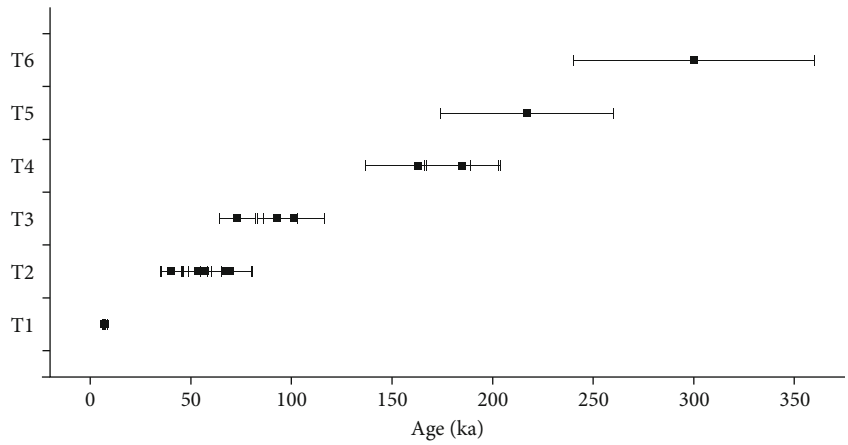

Figure 8: Temporal distribution of all the chronology samples.

Longmen Shan (Figure 2). This may indicate continuous activity in the foreland region. According to seismic profiles (Figure 9(b)), previous studies have proposed that two imbricated, blind thrust faults are developed beneath the front range of the Longmen Shan [35, 36, 40], which has extended into the Sichuan Basin and would affect the densely populated area in the basin (Figure 9(b)). In this study, we also found that the anticlines, which are generated by the upper blind thrust fault, were active during the Late Quaternary (Figure 9(b)).

In some active thrust sheets, active deformation can be quantitatively constrained by utilizing kinematic fault-related folding theories [27–29]. This method requires a suite of well-preserved river terraces that extend across an active fold or fault continuously in order to invoke suitable kinematic folding models [44–47]. However, along the Qingyi River, only terrace T1 was continuously preserved and all other higher terraces were distributed sporadically, which was infeasible for establishing a geometrical model. Another approach to deduce horizontal shortening from a terrace longitudinal profile across a fold is the excess area method that assumes planar conservation of mass [26, 48, 49]. This method has been widely applied in limited situations to deduce regional crustal shortening rate [21, 50, 51]. The excess area method requires that the cross-sectional area of a thrust sheet or of individual

Table 4: Revised ages of all terraces.

Terraces	Samples	Site	Coordinates (WGS 84)	Method	Ages (ka)	Evaluated value (ka)
T1	T1-1	Lushan	30°15′3.03″ 102°49′22.35″	^{14}C	6.8-6.9	7.0 ± 0.3
	T1-2	Lushan	30°15′3.03″ 102°49′22.35″	OSL	7.6 ± 0.9	
	T1-3	Ya'an	30°1′1.39″ 103°2′52.65″	^{14}C	6.8-6.7	
	T1-4	Hongya	29°49′51.77″ 103°25′41.99″	OSL	6.8 ± 0.8	
T2	T2-1	Ya'an	29°59′50.62″ 102°57′23.12″	OSL	40.4 ± 5.0	47.9 ± 3.3
	T2-2	Ya'an	29°59′41.71″ 102°57′11.22″	OSL	40.4 ± 5.6	
	T2-3	Hongya	29°53′53.22″ 103°11′22.71″	OSL	57.1 ± 8.2	
	T2-4	Hongya	29°53′40.60″ 103°11′8.21″	OSL	53.5 ± 7.0	
	T2-5	Hongya	29°53′38.84″ 103°11′8.85″	OSL	69.4 ± 11.2	
	T2-6	Hongya	29°50′47.30″ 103°14′42.90″	OSL	67.5 ± 12.6	
T3	T3-1	Lushan	30°8′32.74″ 102°53′34.05″	OSL	73.1 ± 9.7	97.2 ± 9.1
	/	Ya'an	/	OSL	93.0 ± 10.0[a]	
	T3-2	Hongya	29°50′47.30″ 103°14′42.90″	OSL	101.3 ± 15.1	
T4	T4-1	Lushan	30°9′33.27″ 102°52′22.74″	ESR	163 ± 26	177.6 ± 12.3
	T4-2	Ya'an	29°58′27.24″ 102°58′55.82″	ESR	185 ± 19	
	T4-3	Hongya	29°52′23.12″ 103°20′51.13″	ESR	185 ± 18	
T5	T5-1	Hongya	29°56′18.41″ 103°8′12.93″	ESR	217 ± 43	217 ± 43
T6	T6-1	Ya'an	29°59′14.17″ 102°58′14.17″	ESR	300 ± 60	300 ± 60

[a]One of the T3's ages is quoted from a past study with no coordinates [32].

horizons in a thrust sheet is equal in both their deformed and restored states. Shortening is equal to the vertical gradient in the area of structural relief, such that

$$S = d(\Delta A)/dz, \quad (1)$$

where S is the total crustal shortening, ΔA is the shortening area, which is equal to the excess area in the calculation, and the excess area is always the vertical increase of the stratigraphic area generated by tectonic activity, and dz is the depth of the detachment plane, which controls the bottom boundary of the stratigraphic deformation. Considering the complicated tectonic framework, we individually estimated the excess area (ΔA) and the depth of the detachment (dz) in the following.

4.3.1. Estimation of Excess Area. Deformation of strath surfaces has been recommended to calculate excess area rather than the deposit surface in rapidly uplifting areas, such as the Himalayas [26]. In such areas, both the

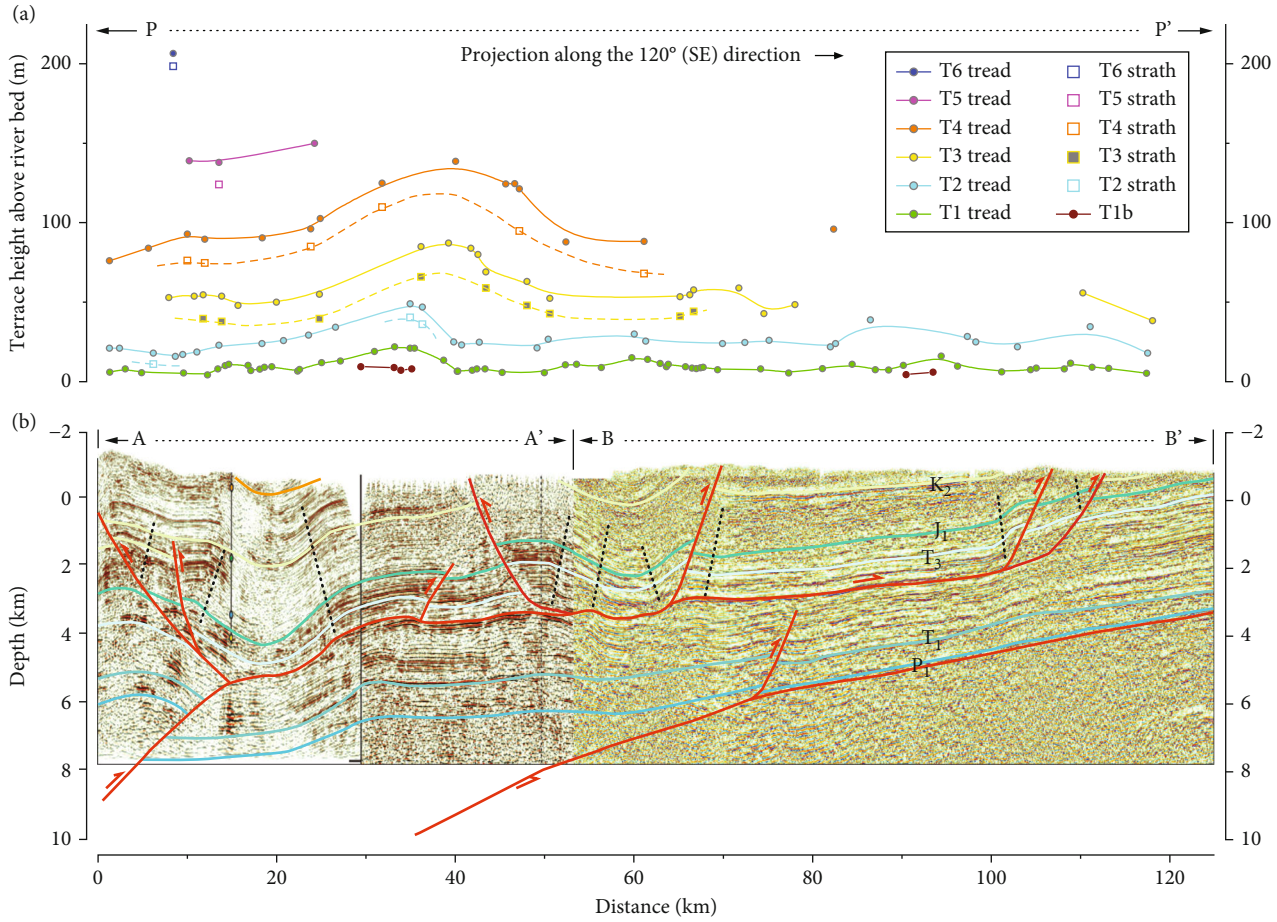

FIGURE 9: Longitudinal profile of Qingyi River terraces, including terraces T1–T6. (a) Deformation of the terrace shown in height above the riverbed (P-P′, position shown in Figure 2), and (b) seismic section of the foreland basin, which is the same with the Figure 3(c).

amount of river incision and river terrace deformation are accounted for in shortening rate calculations because uplifting and tilting are considered to be the dominant patterns of tectonic activity. Additionally, because of the narrow valley and floods, thick silty overlying strata, interpreted as overbank deposits, appeared frequently. Sometimes, these silty deposits could be over 10 m thick. Consequently, terrace surfaces no longer preserved their original heights. Meanwhile, when dealing with fault displacement or fold deformation, well-preserved terrace surfaces were also considered in analyses of deformation [52]. In the Qingyi River basin, terrace straths were not exposed continuously along the river on account of heavy erosion and dense vegetation. A majority of observed straths exhibited lower elevations because of the covering of eroded gravel and vegetation. Meanwhile, the river valleys in the foreland area are so broad that terraces have rarely been influenced by overbank floods. The thickness of the gravel deposits was found to be constant in multiple segments along the river (Table 5). The measured terraces had integrated and dualistic fluvial structures and were determined to have not been reconstructed or flooded. Hence, we used the measured terrace surfaces to estimate the excess area of each terraces in different levels. The excess area was deduced by subtracting the conceivable original riverbed from the area of the deformed terraces (Table 6). As terrace T1b is developed only in the core region of the Xiongpo and Longquanshan anticlines (Figure 9(a)), it was not considered in the excess area calculations.

4.3.2. Estimation of Detachment Depth. According to seismic reflection data, the three anticlines in the foreland region are derived from a shallow detachment with a depth of 3–4 km [9, 53]. However, in the area of the Xiongpo and Sansuchang anticlines, this detachment layer has probably involved into deformation (Figures 3(c) and 3(d)). In this regard, large uncertainties might arise from the estimation when using single-bed excess area. According to seismic reflection data across the whole Sichuan Basin, there are three detachment levels, which define the base of the thrust sheets in the foreland of southern Longmen Shan: a shallow detachment 3–5 km below the surface, an intermediate detachment 5–7 km below the surface, and a deep detachment approximately 15 km deep [5, 54]. Among them, the shallow one controls the current deformation of surficial anticlines, the middle and deep two detachments probably extend to the eastern mountain belt

Table 5: Thickness of the terrace deposits along the Qingyi River in the foreland region.

River basin[a]		Lushan	Ya'an	Caoyutan	Hongya	Jiajiang
Deposit thickness (m)	T1	3.0 ± 0.4	4.5	/	/	/
	T2	8.5 ± 2.0	9.0	8.4 ± 0.6	8.0	/
	T3	12.6 ± 1.3	14.2 ± 1.6	16.0 ± 1.9	15	13.9 ± 2.2
	T4	22.1 ± 2.4	19.9 ± 3.7	23.0 ± 5.2	20.1	/

[a]Locations of each river basin are shown in Figure 10(b).

Table 6: Calculated shortening rate of the anticlines in the foreland region.

Anticline	Terrace	Excess area (km^2)	Detachment depth (km)	Shortening extent (m)	Age (ka)	Shortening rate (mm/yr)
Xiongpo (XPA)	T1	0.0460	3.7-4.0	12.0 ± 1.2	7.0 ± 0.3	1.29 ± 0.11
			7.0-7.9	6.2 ± 0.7		
	T2	0.2240	3.7-4.0	58.2 ± 6.0	47.9 ± 3.3	0.93 ± 0.10
			7.0-7.9	30.0 ± 3.2		
	T3	0.4630	3.7-4.0	120.1 ± 12.4	97.2 ± 9.1	0.95 ± 0.12
			7.0-7.9	62.0 ± 6.6		
	T4	0.8050	3.7-4.0	208.9 ± 21.4	177.6 ± 12.3	0.87 ± 0.09
			7.0-7.9	99.8 ± 12.6		
	Evaluated	/	/	/	/	1.01 ± 0.05
Sansuchang (SSCA)	T3	0.0676	3.2-3.8	19.2 ± 2.2	97.2 ± 9.1	0.16 ± 0.02
			5.5-5.9	11.9 ± 1.2		
Longquanshan (LQSA)	T1	0.0245	3.4-3.8	6.8 ± 0.7	7.0 ± 0.3	0.97 ± 0.11
	T2	0.1403	3.4-3.8	38.9 ± 4.1	47.9 ± 3.3	0.82 ± 0.10
	Evaluated	/	/	/	/	0.89 ± 0.07
Total	/	/	/	/	/	2.06 ± 0.14

in Sichuan Basin (Figure 2(c)). In the foothill and foreland regions, referring to regional seismic profiles (Figure 3(d)), the middle detachment owns a depth of 7 to 10 km and is not deformed [9]. Consequently, we took the shallow detachment (3–4 km) as the minimum value, corresponding to the maximum crustal shortening rate, and the middle detachment (7–10 km) as the maximum value, corresponding to the minimum crustal shortening rate. Against each anticline, the depth of the two detachments was interpreted individually. We used the two detachments to estimate crustal shortening rates of Xiongpo and Sansuchang anticlines and the single shallow detachment to estimate the Longquanshan anticline.

4.3.3. Calculation of Shortening Rate. The local terraces, T5 and T6, are too restricted to reflect tectonic activity. Hence, terraces T1-T4 in the Xiongpo anticline, T3 in the Sansuchang anticline, and T1-T2 in the Longquanshan anticline were used to estimate the shortening rate. Longitudinal profile of terrace's height above the riverbed was integrated along the individual curve to get the excess area (Table 6). The shallow detachment depth was interpreted to be 3.7–4.0 km in the Xiongpo anticline, 3.2–3.8 km in the Sansuchang anticline, and 3.4–3.8 in the Longquanshan anticline. The middle detachment depth was interpreted to be 7.0–7.9 km in the Xiongpo anticline and 5.5–5.9 km in the Sansuchang anticline (Table 6). We assess that the shallow detachment in the Longquanshan anticline is not involved into deformation; hence, a single detachment model was performed.

We applied the Monte Carlo simulation to estimate uncertainties of the increments in the calculating process of chronological data and shortening rate. Our simulations followed the approach of studies that focused on typical fold-related models [27–29]. In our simulations, the probability distributions of each input parameter are sampled randomly for 50000 trials to generate a frequency distribution. Reported values reflect the mode of the output histogram and the associated 95% confidence intervals. Input parameters contain the excess area, detachment depth, and terrace age. Output parameters contain the total shortening length and shortening rate. Details of the Monte Carlo simulation are shown in Supplemental material D.

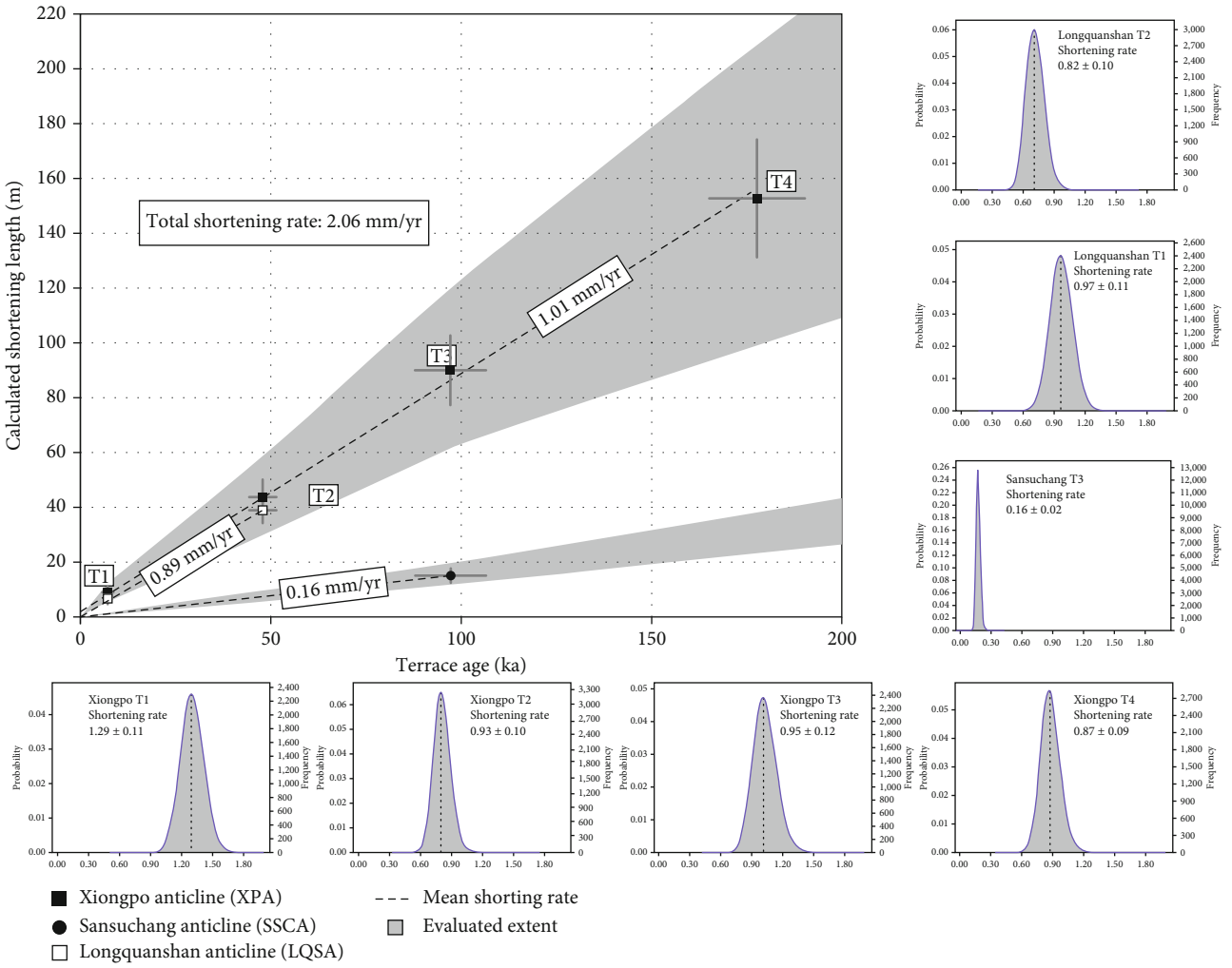

Figure 10: Estimation of the crustal shortening rates of Xiongpo, Sansuchang, and Longquanshan anticlines. Seven terraces, including terrace T1–T4 in Xiongpo anticline, terrace T3 in Sansuchang anticline, and terraces T1–T2 in Longquanshan anticline, were processed by Monte Carlo simulation for 50000 trials. The evaluated extent in summarizing graph represents results from different detachment depths. The slope of the fitting line reflects the final results of shortening rate.

Seven terraces, including terrace T1–T4 in Xiongpo anticline, terrace T3 in Sansuchang anticline, and terraces T1–T2 in Longquanshan anticline, were processed by Monte Carlo simulation for 50000 trials (Figure 10). Then, the overall data were plotted in the summarizing graph to show their characteristics. The Xiongpo and Sansuchang anticline were estimated according to a model with two detachments, and the estimating results were shown as irregular extents in the graph (Figure 10). Moreover, with regard to the Xiongpo and Longquanshan anticline, the trends of the shortening rates that obtained from different level of terraces seem to be continuous and stable (Figure 10). A linear fitting was applied to evaluate the average shortening rate. Consequently, the results showed that the evaluated crustal shortening rates of the Xiongpo anticline, Sansuchang anticline, and Longquanshan anticline are 1.01 ± 0.05 mm/yr, 0.16 ± 0.02 mm/yr, and 0.89 ± 0.07 mm/yr, respectively. We propose that the total crustal shortening rate of the Longmen Shan foreland area is 2.06 ± 0.14 mm/yr.

5. Discussion

5.1. Tectonic Shortening Pattern. From the result of total shortening rate, it can be seen that the Xiongpo anticline accounts for 48%, the Sansuchang anticline accounts for 9%, and the Longquanshan anticline accounts for 43%. The Late Quaternary shortening rate of the southern Longquanshan anticline (0.89 mm/yr) is considerably smaller than that of the northern Longquanshan anticline, which was reported to be 1.47 mm/yr [21]. However, the Xiongpo anticline possesses the largest shortening rate in the foreland area of southern Longmen Shan, which is corresponding to the topography. The extremely small shortening rate of the Sansuchang anticline indicates that the shortening of the foreland is not distributed in-sequence. Considering the serious surficial erosion and low terrain, the activity of the Sansuchang anticline has probably transformed to the Xiongpo anticline. Furthermore, taking the shortening rate of the front range in the southern Longmen Shan

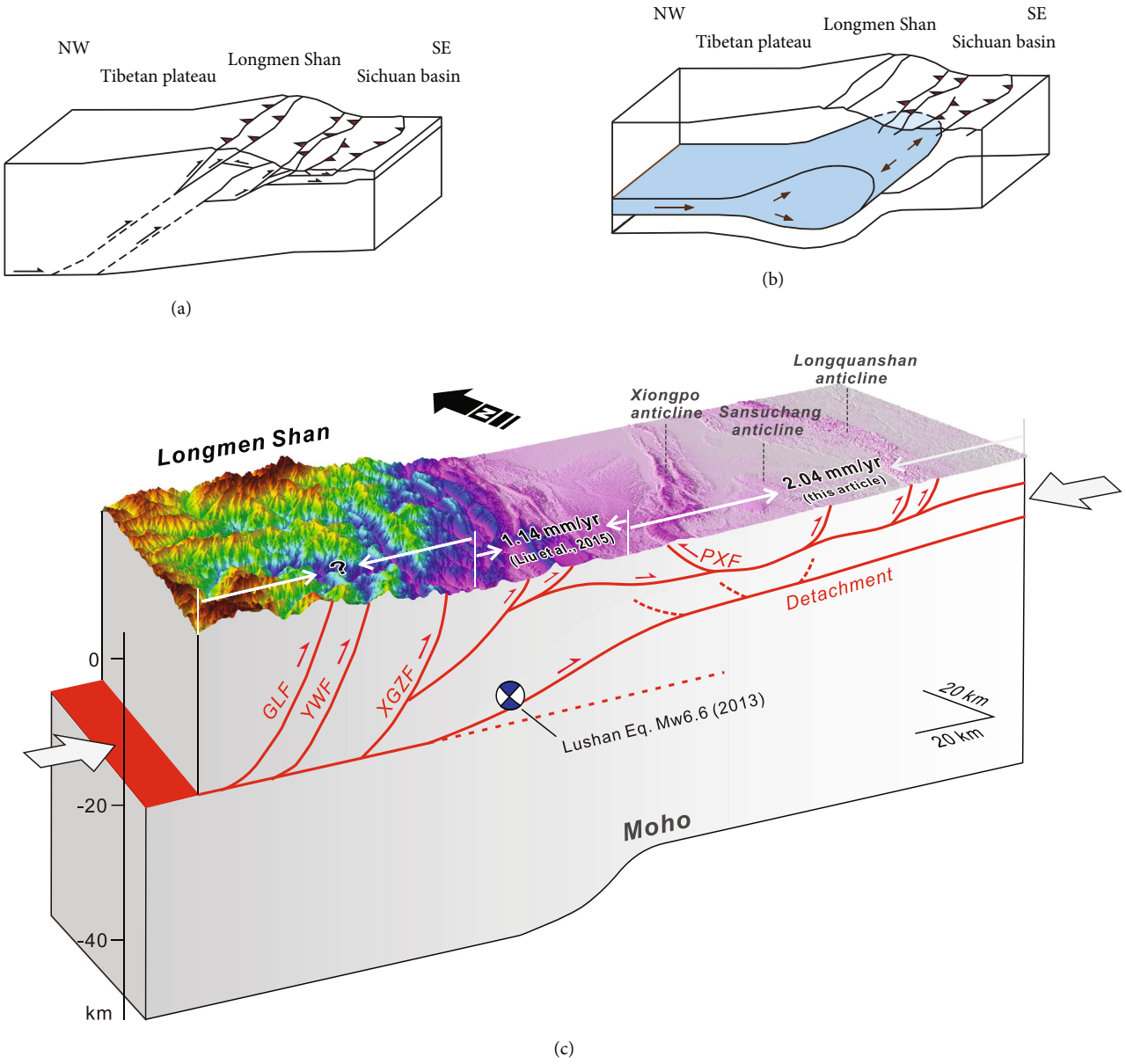

FIGURE 11: Kinetic model of the southern Longmen Shan. Fault sketch follows Hubbard et al., Jia et al., and Wang et al. [5, 9, 59]. Interpretations of the Mohorovičić discontinuity are in reference to seismic reflection profiles [8, 60]. Abbreviations: GLF: Gengda-Longdong fault; XGZF: Xiaoguanzi fault; YWF: Yanjing-Wulong fault.

(1.14 mm/yr) into consideration [32], the overall shortening rate that controlled by the detachment system is assessed to be 3.18 mm/yr, which is 54% higher than that of the northern Longmen Shan.

The SW segment of the Longmen Shan seems to be in a rapidly shortening period, especially the activity of detachments, which has expanded into the foreland basin and sustained strong activity in the Late Quaternary period. We proposed that the 2013 Lushan earthquake ($M_S = 7.0$) may rupture the middle detachment, which has extended into the foreland basin and controlled the surficial deformation (Figure 11(c)). The ramp of the detachment probably acted as a locking structure, which was proved to have been uplifting the surface constantly during the Late Quaternary [32]. Seismic reflection and earthquake relocation data further revealed that a back thrust vertical to the ramp of detachment also ruptured in the Lushan earthquake [55–58]. Overall, a kinetic model shows the tectonic shortening pattern of the southern Longmen Shan: the southern Longmen Shan seems to be an actively reversing edge of the plateau, and the foreland area has absorbed the majority of the shortening (Figure 11(c)). The Late Quaternary shortening rate of the detachment system (3.18 mm/yr) is considerable for the mountain building and foreland expansion. Therefore, our work suggests that, compared to the effect of channel flow (Figure 11(b)), crustal shortening played a leading role in the current uplift of Longmen Shan (Figure 11(a)).

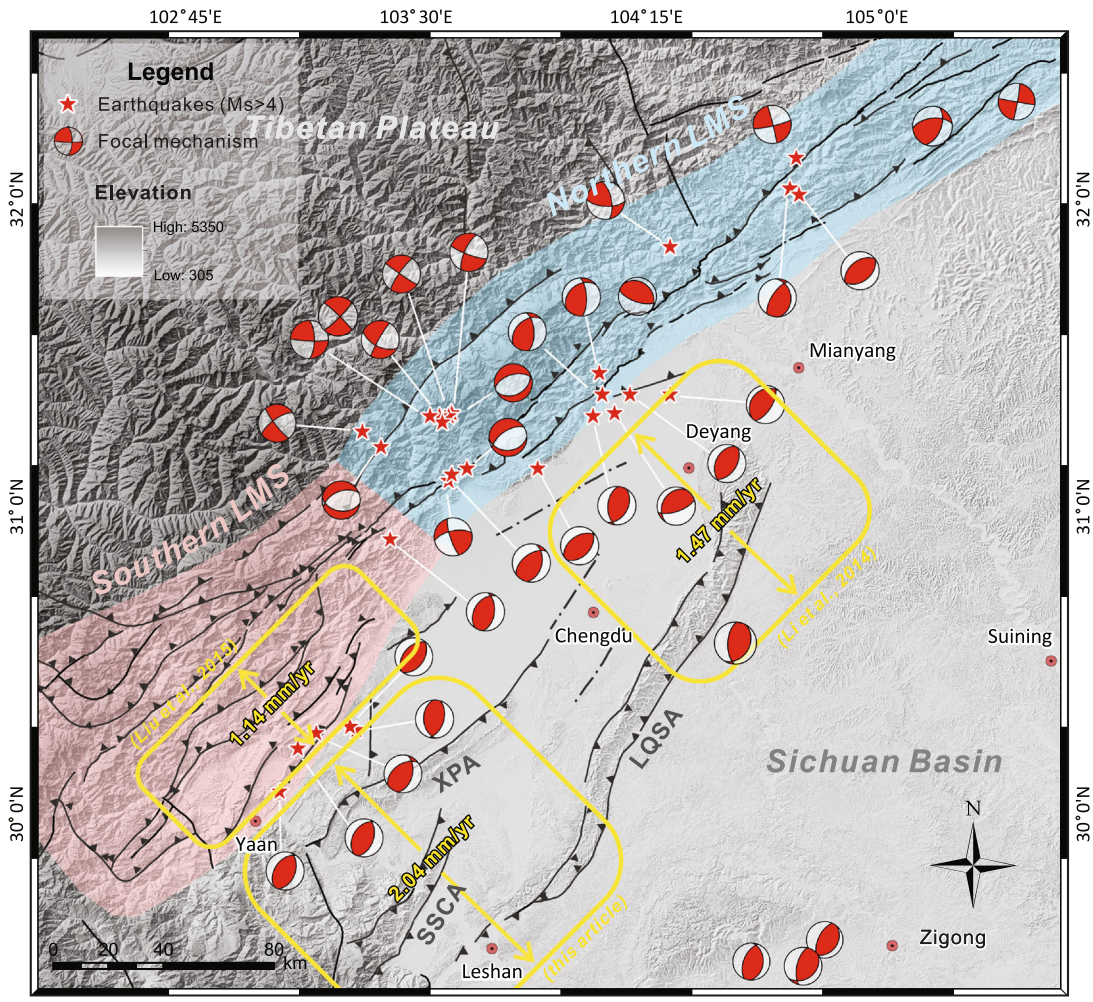

FIGURE 12: Focal mechanism data following the Global CMT Project [61]; data are from earthquakes ($M_S \geq 4.5$) between 2000 and 2021.

5.2. Along-Strike Variation of the Longmen Shan. The along-strike variation is a particular feature of the Longmen Shan. The northern Longmen Shan exhibits a distinctive structural pattern that comprised of three primary active faults. However, the southern segment possesses a broad thrust zone with multiple fault branches and a fold-generated foreland basin (Figure 12). We processed the focal mechanism data to understand the converging characteristics of the belt. Beach balls showing the focal mechanisms of earthquakes ($M_S \geq 4.5$) from 2000 to 2021 were projected on the map (Figure 12). The focal mechanism data were from the Global CMT Project [61]. Each beach ball can be treated as a stereographic projection of the strain ellipse due to the deformation associated with an earthquake. Solid quadrants show orientations of extensional strain, and open quadrants show orientations of compressional strain. In the Longmen Shan, the focal mechanisms in the southern segment can clearly be seen to differ from those in the northern segment (Figure 12). In the northern Longmen Shan, strike-slip is concentrated on the middle region of the belt, as well as the backland; in the frontal region, convergence shows the reversing characteristic that may be generated by a blind fault [9]. In contrast, in the SW, overall convergence is orthogonal to the regional strike and is achieved purely by thrusting.

Previous studies suggested that the reactivation of Triassic structures played an important role in the complex evolution of the Longmen Shan [10]. A "maximum exhumation belt" was proposed to explain the along-strike variation of the Longmen Shan. This belt strikes from the southern Longmen Shan to western Min Shan and was ~15° anticlockwise to the overall Longmen Shan belt. The deviation between the two belts generates the along-strike variation: from south to north along the strike, the reverse slip component on faults, and the uplift rate in the hanging-wall blocks decrease, while the dextral strike-slip component and the corresponding slip rate increase. Our results further verified the deduction of this model. We found that the southern Longmen Shan has an expanding foreland structure, which is dominated by detachment system with a shortening rate of 3.2 mm/yr. On the contrast, the foreland shortening rate in the northern Longmen Shan was limited to 1.47 mm/yr [21], and a part of strain was probably assigned to the transpressional movement of the Beichuan-Yingxiu [62] and Qingchuan faults [63]. Another factor that cannot be ignored is that the upper crust may be decoupled from the middle and lower crust due to the existence of the detachments in the foreland area of the Longmen Shan. Although surface denudation and Moho gradient reflect the trend of

plateau expansion, the surficial deformation may reflect a shallower tectonic pattern and a smaller time-scale deformation.

6. Conclusions

In this article, terrace deformation of the Qingyi River was quantitatively analyzed to estimate the Late Quaternary crustal shortening rate and deformation pattern. A kinetic model was established to explain the deformation pattern and activity distribution of the southern Longmen Shan. Based on our research, the mechanism of orogenic evolution and along-strike variation of the Longmen Shan was further discussed.

By systematic measurement of the terraces in six levels with a net-based RTK approach, we generated a longitudinal profile of Qingyi River across the foreland in the southern Longmen Shan. Among the terraces, terraces T5 and T6 were too restricted to reflect tectonic activity, and terraces T1-T4 in the Xiongpo anticline, T3 in the Sansuchang anticline, and T1-T2 in the Longquanshan anticline were used to estimate the shortening rate. Moreover, by the dating methods of ^{14}C, OSL, and ESR, the chronology sequence of the river terraces was estimated. Namely, the age of terrace T6 is 300 ka; the age of T5 is 217 ka; the age of T4 is 178 ka, while that of T3 is 97 ka, T2 is 48 ka, and T1 is 7 ka.

Excess area method was applied to calculate shortening rate, and Monte Carlo simulation was used to estimate increments in the calculation. The results indicate that the overall Late Quaternary shortening rate of the foreland in the southern Longmen Shan is 2.06 mm/yr, in which the Xiongpo anticline accounts for 48% (1.01 mm/yr), the Longquanshan anticline accounts for 43% (0.89 mm/yr), and the Sansuchang anticline accounts for 9% (0.16 mm/yr). The Xiongpo anticline seems to be the most active structure in the foreland of the southern Longmen Shan, and the Sansuchang anticline has been declined during the Late Quaternary.

According to the shortening rate, we propose that the special fold-generated foreland of the southern Longmen Shan is an expanding segment of the thrust belt and possesses dispersive activities. The active folds are derived from a thin-skinned structure that was dominated by double detachments. The 2013 Lushan earthquake ($M_S = 7.0$) may be related to the ramp of the deeper detachment. In addition, the deformation pattern in this article specifies the along-strike kinematic variation of the Longmen Shan: the southern segment is under the compression of in the NW-SE trend and has a broad deformation belt, while the northern segment has a narrow belt and accommodates the transpressional strain to the dextral strike-slip movement.

Abbreviations

BYF: Beichuan-Yingxiu fault
DTF: Datang fault
GLF: Gengda-Longdong fault
JGF: Jiangyou-Guanxian fault
LQSA: Longquanshan anticline
PXF: Pujiang-Xinjin fault
RTK: Real-time kinematic
SSCA: Sansuchang anticline
WMF: Wenchuan-Maowen fault
XGZF: Xiaoguanzi fault
XPA: Xiongpo anticline
YWF: Yanjing-Wulong fault.

Data Availability

The underlying data is available in the article tables and the appendant tables.

Conflicts of Interest

The authors declare that they have no conflicts of interest.

Acknowledgments

This project has been supported by the National Natural Science Foundation of China (41802226) and the research grants from the National Institute of Natural Hazards, Ministry of Emergency Management of China (grant number ZDJ 2018-03).

Supplementary Materials

The supplementary material includes the outcrops of the dating sample, the calibrated results of 14C dating, the results of OSL dating, the illustration of the Monte Carlo simulations, the results of the classification of terraces, and the RTK data of the field measured terraces. *(Supplementary Materials)*

References

[1] E. Kirby, P. W. Reiners, M. A. Krol et al., "Late Cenozoic evolution of the eastern margin of the Tibetan plateau: inferences from40Ar/39Ar and (U-Th)/He thermochronology," *Tectonics*, vol. 21, no. 1, pp. 1-1–120, 2002.

[2] B. C. Burchfiel, L. H. Royden, R. D. van der Hilst et al., "A geological and geophysical context for the Wenchuan earthquake of 12 may 2008, Sichuan, People's Republic of China," *GSA Today*, vol. 18, no. 7, p. 4, 2008.

[3] A. Yin, "A special issue on the great 12 May 2008 Wenchuan earthquake (M w 7.9): observations and unanswered questions," *Tectonophysics*, vol. 491, no. 1-4, pp. 1–9, 2010.

[4] X. Tan, Y. Liu, Y. Lee et al., "Parallelism between the maximum exhumation belt and the Moho ramp along the eastern Tibetan plateau margin: coincidence or consequence?," *Science Letters*, vol. 507, pp. 73–84, 2019.

[5] J. Hubbard and J. H. Shaw, "Uplift of the Longmen Shan and Tibetan plateau, and the 2008 Wenchuan (M=7.9) earthquake," *Nature*, vol. 458, no. 7235, pp. 194–197, 2009.

[6] Y. Tian, B. P. Kohn, A. J. W. Gleadow, and S. Hu, "Constructing the Longmen Shan eastern Tibetan plateau margin: insights from low-temperature thermochronology," *Tectonics*, vol. 32, no. 3, pp. 576–592, 2013.

[7] Y. Zhou, Z. Wu, Y. Sun, G. C. Wang, and J. L. Wang, "Constraints on Late Cenozoic tectonics in the southern Longmen Shan: evidence from low-temperature thermochronology,"

International Geology Review, vol. 63, no. 13, pp. 1619–1633, 2021.

[8] X. Guo, R. Gao, G. R. Keller, X. Xu, H. Wang, and W. Li, "Imaging the crustal structure beneath the eastern Tibetan plateau and implications for the uplift of the Longmen Shan range," *Earth and Planetary Science Letters*, vol. 379, pp. 72–80, 2013.

[9] D. Jia, Y. Li, A. Lin et al., "Structural model of 2008 M-w 7.9 Wenchuan earthquake in the rejuvenated Longmen Shan thrust belt, China," *Tectonophysics*, vol. 491, no. 1-4, pp. 174–184, 2010.

[10] M. Sun, A. Yin, D. Yan et al., "Role of pre-existing structures in controlling the Cenozoic tectonic evolution of the eastern Tibetan plateau: new insights from analogue experiments," *Earth and Planetary Science Letters*, vol. 491, pp. 207–215, 2018.

[11] B. C. Burchfiel, Z. Chen, Y. Liu, and L. H. Royden, "Tectonics of the Longmen Shan and adjacent regions, Central China," *International Geology Review*, vol. 37, no. 8, pp. 661–735, 1995.

[12] M. K. Clark and L. H. Royden, "Topographic ooze: building the eastern margin of Tibet by lower crustal flow," *Geology*, vol. 28, no. 8, pp. 703–706, 2000.

[13] A. Robert, M. Pubellier, J. de Sigoyer et al., "Structural and thermal characters of the Longmen Shan (Sichuan, China)," *Tectonophysics*, vol. 491, no. 1-4, pp. 165–173, 2010.

[14] X. D. Jiang and Y. Jin, "Mapping the deep lithospheric structure beneath the eastern margin of the Tibetan plateau from gravity anomalies," *Earth*, vol. 110, no. B7, 2005.

[15] X. Tan, X. Xu, Y. Lee et al., "Late Cenozoic thrusting of major faults along the central segment of Longmen Shan, eastern Tibet: evidence from low-temperature thermochronology," *Tectonophysics*, vol. 712-713, pp. 145–155, 2017.

[16] R. Lu, D. He, S. John, J. E. Wu, B. Liu, and Y. Chen, "Structural model of the central Longmen Shan thrusts using seismic reflection profiles: implications for the sediments and deformations since the Mesozoic," *Tectonophysics*, vol. 630, pp. 43–53, 2014.

[17] X. Xu, X. Wen, G. Yu et al., "Coseismic reverse- and oblique-slip surface faulting generated by the 2008 Mw 7.9 Wenchuan earthquake, China," *Geology*, vol. 37, no. 6, pp. 515–518, 2009.

[18] Z. Ren, Z. Zhang, F. Dai, J. Yin, and H. Zhang, "Topographic changes due to the 2008 mw 7.9 Wenchuan earthquake as revealed by the differential DEM method," *Geomorphology*, vol. 217, pp. 122–130, 2014.

[19] X. Xu, X. Wen, Z. Han et al., "Lushan M S7. 0 earthquake: a blind reserve-fault event," *Chinese Science Bulletin*, vol. 58, no. 28-29, pp. 3437–3443, 2013.

[20] W. Zheng, W. Wang, C. Li, Z. We, and X. Ga, "The deformation of the Xiongpo anticline and the activity of Pujiang-xinjin fault," *Seismology and Geology*, vol. 30, no. 4, pp. 957–967, 2008.

[21] K. Li, X. Xu, X. Tan, G. H. Chen, C. Xu, and W. J. Kang, "Late Quaternary deformation of the Longquan anticline in the Longmenshan thrust belt, eastern Tibet, and its tectonic implication," *Journal of Asian Earth Sciences*, vol. 112, pp. 1–10, 2015.

[22] W. Wang, L. Zhao, J. Li, and Z. Yao, "Rupture process of the Ms 8.0 Wenchuan earthquake of Sichuan, China," *Chinese Journal of Geophysics*, vol. 51, no. 5, pp. 1403–1410, 2008.

[23] W. Wang, J. Hao, and Z. Yao, "Preliminary result for rupture process of Apr. 20, 2013, Lushan earthquake, Sichuan, China," *Chinese Journal of Geophysics*, vol. 56, no. 4, pp. 1412–1417, 2013.

[24] W. Gan, P. Zhang, Z. Shen et al., "Present-day crustal motion within the Tibetan plateau inferred from GPS measurements," *Journal of Geophysical Research*, vol. 112, no. B8, 2007.

[25] E. Kirby, K. X. Whipple, W. Tang, and Z. Chen, "Distribution of active rock uplift along the eastern margin of the Tibetan plateau: inferences from bedrock channel longitudinal profiles," *Journal of Geophysical Research: Solid Earth*, vol. 108, no. B4, p. 2217, 2003.

[26] J. Lavé and J. P. Avouac, "Active folding of fluvial terraces across the Siwaliks Hills, Himalayas of Central Nepal," *Journal of Geophysical Research: Solid Earth*, vol. 105, no. B3, pp. 5735–5770, 2000.

[27] T. Li, J. Chen, J. A. Thompson, D. W. Burbank, and X. Yang, "Quantification of three-dimensional folding using fluvial terraces: a case study from the Mushi anticline, northern margin of the Chinese Pamir," *Journal of Geophysical Research: Solid Earth*, vol. 118, no. 8, pp. 4628–4647, 2013.

[28] C. B. Amos, D. W. Burbank, D. C. Nobes, and S. A. L. Read, "Geomorphic constraints on listric thrust faulting: implications for active deformation in the Mackenzie Basin, South Island, New Zealand," *Journal of Geophysical Research: Solid Earth*, vol. 112, no. B3, pp. B3S–B11S, 2007.

[29] S. C. Thompson, R. J. Weldon, C. M. Rubin, K. Abdrakhmatov, P. Molnar, and G. W. Berger, "Late Quaternary slip rates across the central Tien Shan, Kyrgyzstan, Central Asia," *Journal of Geophysical Research: Solid Earth*, vol. 107, no. B9, pp. ETG 7-1–ETG 7-32, 2002.

[30] T. Parsons, C. Ji, and E. Kirby, "Stress changes from the 2008 Wenchuan earthquake and increased hazard in the Sichuan basin," *Nature*, vol. 454, no. 7203, pp. 509-510, 2008.

[31] Z. Ren and A. Lin, "Co-seismic landslides induced by the 2008 Wenchuan magnitude 8.0 earthquake, as revealed by ALOS PRISM and AVNIR2 imagery data," *International Journal of Remote Sensing*, vol. 31, no. 13, pp. 3479–3493, 2010.

[32] S. Liu, S. Zhang, R. Ding et al., "Upper crustal folding of the 2013 Lushan earthquake area in southern Longmen Shan, China, insights from Late Quaternary fluvial terraces," *Tectonophysics*, vol. 639, pp. 99–108, 2015.

[33] Z. Li, P. Zhang, W. Zheng et al., "Oblique thrusting and strain partitioning in the Longmen Shan fold-and-thrust belt, eastern Tibetan plateau," *Journal of Geophysical Research: Solid Earth*, vol. 123, no. 5, pp. 4431–4453, 2018.

[34] M. Wang and A. Lin, "Active thrusting of the Longquan fault in the Central Sichuan basin, China, and the seismotectonic behavior in the Longmen Shan fold-and-thrust belt," *Journal of Geophysical Research: Solid Earth*, vol. 122, no. 7, pp. 5639–5662, 2017.

[35] D. Jia, G. Wei, Z. Chen, B. Li, Q. Zeng, and G. Yang, "Longmen Shan fold-thrust belt and its relation to the western Sichuan Basin in Central China: new insights from hydrocarbon exploration," *AAPG Bulletin*, vol. 90, no. 9, pp. 1425–1447, 2006.

[36] Y. Li, D. Jia, J. H. Shaw et al., "Structural interpretation of the coseismic faults of the Wenchuan earthquake: three-dimensional modeling of the Longmen Shan fold-and-thrust belt," *Journal of Geophysical Research*, vol. 115, no. B4, 2010.

[37] P. Zhang, X. Wen, Z. Shen, and J. H. Chen, "Oblique, high-angle, listric-reverse faulting and associated development of strain: the Wenchnan earthquake of May 12, 2008, Sichuan, China," *Annual Review of Earth and Planetary Sciences*, vol. 38, pp. 353–382, 2010.

[38] Z. Li, W. Zheng, P. Zhang et al., "Evidence for three Cenozoic phases of upper crustal shortening of the Xiongpo structure in the Longmen Shan fold-and-thrust belt, China: implications for the eastward growth of the eastern Tibetan plateau," *Journal of Asian Earth Sciences*, vol. 179, pp. 138–148, 2019.

[39] M. Wang, D. Jia, J. H. Shaw et al., "Active fault-related folding beneath an alluvial terrace in the southern Longmen Shan range front, Sichuan basin, China: implications for seismic hazard," *Bulletin of the Seismological Society of America*, vol. 103, no. 4, pp. 2369–2385, 2013.

[40] M. Wang, D. Jia, J. H. Shaw et al., "The 2013 Lushan earthquake: implications for seismic hazards posed by the range front blind thrust in the Sichuan Basin, China," *Geology*, vol. 42, no. 10, pp. 915–918, 2014.

[41] C. B. Ramsey and S. Lee, "Recent and planned developments of the program OxCal," *Radiocarbon*, vol. 55, no. 2, pp. 720–730, 2013.

[42] Y. C. Lu, X. L. Wang, and A. G. Wintle, "A new OSL chronology for dust accumulation in the last 130,000 yr for the Chinese loess plateau," *Quaternary Research*, vol. 67, no. 1, pp. 152–160, 2007.

[43] D. Jiang, S. Zhang, and W. Li, "Research on the quaternary fluvial geomorphological surface sequence of the foreland region in southern Longmen Shan, eastern Tibet," *Geomorphology*, vol. 269, pp. 133–148, 2016.

[44] J. M. Stockmeyer, J. H. Shaw, N. D. Brown et al., "Active thrust sheet deformation over multiple rupture cycles; a quantitative basis for relating terrace folds to fault slip rates," *Geological Society of America Bulletin*, vol. 129, no. 9-10, pp. 1337–1356, 2017.

[45] H. Yang, X. Yang, H. Zhang, X. Huang, W. Huang, and N. Zhang, "Active fold deformation and crustal shortening rates of the Qilian Shan foreland Thrust Belt, NE Tibet, since the Late Pleistocene," *Tectonophysics*, vol. 742-743, pp. 84–100, 2018.

[46] A. Hubert-Ferrari, J. Suppe, R. Gonzalez-Mieres, and X. Wang, "Mechanisms of active folding of the landscape (southern Tian Shan, China)," *Journal of Geophysical Research: Solid Earth*, vol. 112, no. B3, pp. B3S–B9S, 2007.

[47] C. B. Amos, D. W. Burbank, and S. A. Read, "Along-strike growth of the Ostler fault, New Zealand: consequences for drainage deflection above active thrusts," *Tectonics*, vol. 29, no. 4, 2010.

[48] R. Gonzalez-Mieres and J. Suppe, "Relief and shortening in detachment folds," *Journal of Structural Geology*, vol. 28, no. 10, pp. 1785–1807, 2006.

[49] D. Saint-Carlier, J. Charreau, J. Lavé et al., "Major temporal variations in shortening rate absorbed along a large active fold of the southeastern Tianshan piedmont (China)," *Earth and Planetary Science Letters*, vol. 434, pp. 333–348, 2016.

[50] P. Su, H. He, Z. Wei et al., "A new shortening rate across the Dushanzi anticline in the northern Tian Shan Mountains, China from lidar data and a seismic reflection profile," *Journal of Asian Earth Sciences*, vol. 163, pp. 131–141, 2018.

[51] W. Huang, X. Yang, A. Li et al., "Late Pleistocene shortening rate on the northern margin of the Yanqi Basin, southeastern Tian Shan, NW China," *Journal of Asian Earth Sciences*, vol. 112, pp. 11–24, 2015.

[52] Y. Chen, J. Hung, K. Lai, Y. N. N. Lin, T. Wilcox, and K. Mueller, "River terrace development in response to folding above active wedge thrusts in Houli, Central Taiwan," *Journal of Asian Earth Sciences*, vol. 31, no. 3, pp. 240–250, 2007.

[53] Z. Li, D. Jia, W. Chen et al., "Late Cenozoic east-west crustal shortening in southern Longmen Shan, eastern Tibet: implications for regional stress field changes," *Tectonophysics*, vol. 623, pp. 169–186, 2014.

[54] J. Hubbard, J. H. Shaw, and Y. Klinger, "Structural setting of the 2008 M-w 7.9 Wenchuan, China, Earthquake," *Bulletin of the Seismological Society of America*, vol. 100, no. 5B, pp. 2713–2735, 2010.

[55] Z. Li, J. Liu-Zeng, R. Almeida, J. Hubbard, C. Sun, and G. Yi, "Re-evaluating seismic hazard along the southern Longmen Shan, China: insights from the 1970 Dayi and 2013 Lushan earthquakes," *Tectonophysics*, vol. 717, pp. 519–530, 2017.

[56] R. Lu, X. Xu, D. He et al., "Seismotectonics of the 2013 Lushan Mw 6.7 earthquake: inversion tectonics in the eastern margin of the Tibetan plateau," *Geophysical Research Letters*, vol. 44, no. 16, pp. 8236–8243, 2017.

[57] G. H. Zhang, E. A. Hetland, X. J. Shan et al., "Triggered slip on a back reverse fault in the Mw6.8 2013 Lushan, China earthquake revealed by joint inversion of local strong motion accelerograms and geodetic measurements," *Tectonophysics*, vol. 672-673, pp. 24–33, 2016.

[58] Y. Li, D. Jia, M. Wang et al., "Structural geometry of the source region for the 2013 mw 6.6 Lushan earthquake: implication for earthquake hazard assessment along the Longmen Shan," *Earth and Planetary Science Letters*, vol. 390, pp. 275–286, 2014.

[59] M. Wang, D. Jia, A. Lin, L. Shen, G. Rao, and Y. Li, "Late Holocene activity and historical earthquakes of the Qiongxi thrust fault system in the southern Longmen Shan fold-and-thrust belt, eastern Tibetan plateau," *Tectonophysics*, vol. 584, no. SI, pp. 102–113, 2013.

[60] H. Li, W. Su, C. Wang, and Z. Huang, "Ambient noise Rayleigh wave tomography in western Sichuan and eastern Tibet," *Earth and Planetary Science Letters*, vol. 282, no. 1-4, pp. 201–211, 2009.

[61] A. M. Dziewonski, T. Chou, and J. H. Woodhouse, "Determination of earthquake source parameters from waveform data for studies of global and regional seismicity," *Journal of Geophysical Research: Solid Earth*, vol. 86, no. B4, pp. 2825–2852, 1981.

[62] H. Wang, H. Li, C. Janssen, Z. Sun, and J. Si, "Multiple generations of pseudotachylyte in the Wenchuan fault zone and their implications for coseismic weakening," *Journal of Structural Geology*, vol. 74, pp. 159–171, 2015.

[63] H. Sun, H. He, Y. Ikeda et al., "Holocene paleoearthquake history on the Qingchuan fault in the northeastern segment of the Longmenshan thrust zone and its implications," *Tectonophysics*, vol. 660, pp. 92–106, 2015.